学 会 等 発 表 実 績

委託業務項目「プリオノイド蛋白質の伝播阻害による治療法開発」

東北大学医学系研究科　長谷川 隆文

1．学会等における口頭・ポスター発表

発表した成果（発表題目、口頭・ポスター発表の別）	発表者氏名	発表した場所（学会等名）	発表した時期	国内・外の別
Retromer dysfunction as an emerging mechanisms of Parkinson's disease（口頭）	長谷川隆文	横浜（第 37 回日本神経科学大会）	2014.9.13	国内
Functional ESCRT machinery is required for the clearance of aggregate-prone proteins associated with neurodegenerative diseases（ポスター）	長谷川隆文	パタヤ、タイ（4th Asian and Oceanian Parkinson's Disease and Movement Disorders Congress）	2014.11.28	国外
How does exogenous alpha-synuclein get access to the endogenous alpha-synuclein proteins?（口頭）	長谷川隆文	インスブルク、オーストリア（MDS course Alpha-Synuclein: The Gateway to Parkinsonism）	2015.2.12	国外

2．学会誌・雑誌等における論文掲載

掲載した論文（発表題目）	発表者氏名	発表した場所（学会誌・雑誌等名）	発表した時期	国内・外の別
Neural Substrates of Cognitive Subtypes in Parkinson's Disease: A 3-Year Longitudinal Study.	Shoji Y, Nishio Y, Baba T, Uchiyama M, Yokoi K, Ishioka T, Hosokai Y, Hirayama K, Fukuda H, Aoki M, Hasegawa T, Takeda A, Mori E.	PLoS One	9(10), e110547, (2014).	国外
VPS35 dysfunction impairs lysosomal degradation of α-synuclein and exacerbates neurotoxicity in a Drosophila model of Parkinson's disease.	Miura E, Hasegawa T, Konno M, Suzuki M, Sugeno N, Fujikake N, Geisler S, Tabuchi M, Oshima R, Kikuchi A, Baba T, Wada K, Nagai Y, Takeda A, Aoki M.	Neurobiol Dis	71:1-13 (2014)	国外
Lys-63-linked Ubiquitination by E3 Ubiquitin Ligase Nedd4-1 Facilitates Endosomal Sequestration of Internalized α-Synuclein.	Sugeno N, Hasegawa T, Tanaka N, Fukuda M, Wakabayashi K, Oshima R, Konno M, Miura E, Kikuchi A, Baba T, Anan T, Nakao M, Geisler S, Aoki M, Takeda A.	J Biol Chem	289: 18137-51 (2014)	国外

学 会 等 発 表 実 績

委託業務項目「プリオノイド蛋白質の高感度検出による疾患バイオマーカー開発」

京都府立医科大学大学院医学研究科　徳田 隆彦

1．学会等における口頭・ポスター発表

発表した成果（発表題目、口頭・ポスター発表の別）	発表者氏名	発表した場所（学会等名）	発表した時期	国内・外の別
Biochemical biomarkers for Parkinson's disease and related disorders、口頭	Tokuda T	13th International Parkinson's Disease Symposium in Takamatsu、高松	2014.2.22	国内
Which biomarkers may be useful as objective outcome measures for clinical trials?、口頭	Tokuda T	18th International Congress of Parkinson's Disease and Movement Disorders、Stockholm	2014.6.12	国外
神経疾患をバイオマーカーで診断？、口頭	徳田隆彦	第 44 回新潟神経学夏期セミナー、新潟	2014.8.2	国内
Extracellular α-synuclein species: usefulness as a biomarker for Parkinson's disease, and their degradation system、口頭	Tokuda T	The 37th Annual Meeting of the Japan Neuroscience Society、横浜	2014.9.13	国内
α-Synuclein is present as a monomer in CSF、ポスター	Tatebe H, Tokuda T, Ishi R, Kasai T, Mizuno T	The 37th Annual Meeting of the Japan Neuroscience Society、横浜	2014.9.13	国内
[F-18]-FDDNP-PET によるパーキンソン症候群の鑑別診断、ポスター	徳田隆彦, 近藤正樹, 松島成典, 水野敏樹, 中川正法	日本認知症学会学術集会(第 33 回)、横浜	2014.12.1	国内

2．学会誌・雑誌等における論文掲載

掲載した論文（発表題目）	発表者氏名	発表した場所（学会誌・雑誌等名）	発表した時期	国内・外の別
Increased α-synuclein levels in the cerebrospinal fluid of patients with Creutzfeldt-Jakob disease.	Kasai T, Tokuda T, Ishii R, Ishigami N, Tsuboi Y, Nakagawa M, Mizuno T, El-Agnaf OMA	J Neurol	2014.6	国外
Lysosomal enzyme cathepsin B enhances the aggregate forming activity of exogenous α-synuclein fibrils.	Tsujimura A, Taguchi K, Watanabe Y, Tatebe H, Tokuda T, Mizuno T, Tanaka M	Neurobiol Dis	2014.1	国外
Decrease in plasma levels of α-synuclein is evident in patients with parkinson's disease after elimination of heterophilic antibody interference.	Ishii R, Tokuda T, Tatebe H, Ohmichi T, Kasai T, Nakagawa M, Mizuno T, El-Agnaf OMA	PLoS ONE	2015(in press)	国外

研究成果の刊行物・別刷

THE JOURNAL OF BIOLOGICAL CHEMISTRY VOL. 290, NO. 3, pp. 1442–1453, January 16, 2015

p62 Plays a Protective Role in the Autophagic Degradation of Polyglutamine Protein Oligomers in Polyglutamine Disease Model Flies*

Received for publication, June 20, 2014, and in revised form, November 26, 2014 Published, JBC Papers in Press, December 5, 2014, DOI 10.1074/jbc.M114.590281

Yuji Saitoh[‡§¶], Nobuhiro Fujikake[‡], Yuma Okamoto[‡], H. Akiko Popiel[‡], Yusuke Hatanaka[‡], Morio Ueyama[‡], Mari Suzuki[‡], Sébastien Gaumer[‖], Miho Murata[§¶], Keiji Wada[‡], and Yoshitaka Nagai[‡1]**

*From the [‡]Department of Degenerative Neurological Diseases, National Institute of Neuroscience, National Center of Neurology and Psychiatry, 4-1-1 Ogawa-Higashi, Kodaira, Tokyo 187-8502, Japan, the [§]Department of Neurology, National Center Hospital, National Center of Neurology and Psychiatry, 4-1-1 Ogawa-higashi, Kodaira, Tokyo 187-8551, Japan, the [¶]Graduate School of Medical and Pharmaceutical Sciences, Chiba University, 1-8-1, Inohana, Chuo-ku, Chiba, Chiba 260-8670, Japan, the [‖]Laboratoire de Génétique et Biologie Cellulaire, EA4589, Université de Versailles-Saint-Quentin-en-Yvelines, École Pratique des Hautes Etudes, 45 Avenue des Etats-Unis, 78035 Versailles Cedex, France, and **Core Research for Evolutional Science and Technology (CREST), Japan Science and Technology Agency, Kawaguchi, Saitama 332-0012, Japan*

Background: Oligomers of pathogenic proteins are implicated in the pathomechanisms of neurodegenerative diseases.
Results: Depletion of p62 delays the degradation of polyglutamine protein oligomers via autophagy and exacerbates neurodegeneration in polyglutamine disease model flies.
Conclusion: p62 plays a protective role via autophagic degradation of polyglutamine protein oligomers.
Significance: p62 should be a therapeutic target for the polyglutamine diseases.

Oligomer formation and accumulation of pathogenic proteins are key events in the pathomechanisms of many neurodegenerative diseases, such as Alzheimer disease, ALS, and the polyglutamine (polyQ) diseases. The autophagy-lysosome degradation system may have therapeutic potential against these diseases because it can degrade even large oligomers. Although p62/sequestosome 1 plays a physiological role in selective autophagy of ubiquitinated proteins, whether p62 recognizes and degrades pathogenic proteins in neurodegenerative diseases has remained unclear. In this study, to elucidate the role of p62 in such pathogenic conditions *in vivo*, we used *Drosophila* models of neurodegenerative diseases. We found that p62 predominantly co-localizes with cytoplasmic polyQ protein aggregates in the MJDtr-Q78 polyQ disease model flies. Loss of p62 function resulted in significant exacerbation of eye degeneration in these flies. Immunohistochemical analyses revealed enhanced accumulation of cytoplasmic aggregates by *p62* knockdown in the MJDtr-Q78 flies, similarly to knockdown of autophagy-related genes (*Atgs*). Knockdown of both *p62* and *Atgs* did not show any additive effects in the MJDtr-Q78 flies, implying that p62 function is mediated by autophagy. Biochemical analyses showed that loss of p62 function delays the degradation of the MJDtr-Q78 protein, especially its oligomeric species. We also found that loss of p62 function exacerbates eye degeneration in another polyQ disease fly model as well as in ALS model flies. We therefore conclude that p62 plays a protective role against polyQ-induced neurodegeneration, by the autophagic degradation of polyQ protein oligomers *in vivo*, indicating its therapeutic potential for the polyQ diseases and possibly for other neurodegenerative diseases.

The polyglutamine (polyQ)[2] diseases are inherited intractable neurodegenerative diseases, including Huntington disease, several spinocerebellar ataxias (SCA1, -2, -6, -7, and -17 and SCA3/MJD), dentatorubral-pallidoluysian atrophy, and spinobulbar muscular atrophy, which are caused by the expansion of a CAG repeat encoding for polyQ stretch within specific genes (1). PolyQ proteins are prone to misfold, oligomerize, and form aggregates and eventually accumulate as inclusion bodies in affected neurons (2, 3). Whereas the formation of polyQ protein inclusion bodies is believed to be protective, by sequestering the toxic polyQ proteins (4), the intermediate structures formed during the aggregation process, such as monomers or oligomers, are reported to be more toxic for the cells, leading to neuronal dysfunction or neuronal cell death (5, 6). The polyQ diseases are thus considered as one of the protein-folding diseases, together with Alzheimer disease, Parkinson disease, and ALS. Because there are currently no effective therapies for the polyQ diseases, establishment of a novel therapy based on the

* This work was supported in part by Grants-in-Aid for Scientific Research (B) (to Y. N.) from the Japan Society for the Promotion of Science (JSPS), Japan; by Grants-in-Aid for Scientific Research on Priority Areas (Proteolysis) (to Y. N.) and on Innovative Areas (Synapse and Neurocircuit Pathology) (to Y. N.) from the Ministry of Education, Culture, Sports, Science, and Technology, Japan; by Health Labor Sciences Research Grants for Research on Development of New Drugs and the Research Committee for Ataxic Diseases (to Y. N.) from the Ministry of Health, Labor, and Welfare, Japan; and by a grant from Core Research for Evolutional Science and Technology (CREST) of the Japan Science and Technology Agency (to Y. N.).

[1] To whom correspondence should be addressed: Dept. of Degenerative Neurological Diseases, National Institute of Neuroscience, National Center of Neurology and Psychiatry, 4-1-1 Ogawa-Higashi, Kodaira, Tokyo 187-8502, Japan. Tel.: 81-42-346-1715; Fax 81-42-346-1745; E-mail: nagai@ncnp.go.jp.

[2] The abbreviations used are: polyQ, polyglutamine; UPS, ubiquitin-proteasome system; MJDtr, truncated form of mutant MJD; IR, inverted repeat RNA; Aβ, amyloid-β; AGE, agarose gel electrophoresis; SEM, scanning electron microscopic.

disease pathomechanism is a challenging theme. Considering the pathomechanism of the polyQ diseases, the clearance of toxic forms of the polyQ proteins should be a promising therapeutic strategy.

Although the precise mechanisms of how polyQ proteins are degraded in the cell are not clearly understood, the two major cellular degradation systems (*i.e.* the autophagy-lysosome system and the ubiquitin-proteasome system (UPS)) are both thought to be involved in polyQ protein degradation (7). However, the UPS may be inadequate for degrading polyQ protein oligomers or aggregates, because substrate proteins of the UPS need to be unfolded when entering the narrow proteasomal pore (8). Furthermore, the mammalian UPS might not have a protease activity to efficiently degrade the polyQ stretch (9, 10). Alternatively, autophagy can degrade even large aggregates by sequestering and delivering them to the lysosome (11). Although autophagy was considered a non-selective degradation system in the past, emerging evidence suggests that it can specifically degrade some ubiquitinated proteins, organelles, and intracellular pathogens; this is now known as "selective autophagy" (12). The specific autophagic degradation of polyQ proteins, including large sized aggregates, would be a preferable therapeutic strategy, because nonspecific degradation of cytosolic proteins may cause adverse effects due to the loss of normal protein functions.

The p62/sequestosome 1 protein (hereafter called p62) was initially identified as an adaptor molecule for the selective autophagic degradation of ubiquitinated proteins, because p62 has domains that bind both ubiquitinated proteins and autophagosomes, giving selectivity to autophagy (13, 14). Neuropathological studies revealed that p62 co-localizes with ubiquitin-positive inclusions consisting of disease-causative proteins within neurons and glia of patients with various neurodegenerative diseases (15, 16). This evidence suggests that p62 is associated with various abnormal proteins, including the polyQ protein. However, whether p62 recognizes these pathogenic proteins as substrates for p62-associated selective autophagy has remained unclear.

In this study, we explored the role of p62 in the polyQ diseases, using *Drosophila* polyQ disease models. We demonstrated that p62 plays an important role in the autophagic degradation of polyQ protein oligomers, resulting in protection against polyQ protein toxicity *in vivo*. Furthermore, we demonstrated the protective role of p62 in various neurodegenerative disease models, indicating that p62 could be a therapeutic target for various neurodegenerative diseases.

EXPERIMENTAL PROCEDURES

Fly Stocks—Flies were raised and maintained on standard cornmeal-agar-yeast-based food at 25 °C. The transgenic fly lines bearing the *gmr-GAL4* (17) or *UAS*-human *TDP-43*[3] transgene have been described previously. The transgenic fly lines bearing the *gmr-GeneSwitch* or *gmr-grim* transgene and the mutant fly line bearing the $Atg6^{00096}$ mutation were obtained from the Bloomington *Drosophila* Stock Center. The transgenic fly lines bearing the *UAS-MJDtr-Q78* and *UAS-MJDtr-Q27* transgene were gifts from Drs. N. M. Bonini (18), and the *UAS-Httex1p97QP* (19), *UAS-Aβ arc2* (20), and *UAS-R406W tau* (21) transgene were gifts from J. L. Marsh, D. C. Crowther, and M. B. Feany, respectively. The mutant fly lines bearing a *ref(2)P* mutation, namely $ref(2)P^{od2}$ or $ref(2)P^{od3}$, were described previously (22). The RNAi fly lines bearing the *UAS-ref(2)P-IR*, *UAS-Atg12-IR*, *UAS-alfy-IR*, or *UAS-Prosβ2-IR* transgene were obtained from the Vienna *Drosophila* Resource Center.

Fly Eye Imaging—Light microscopic images were taken using a stereoscopic microscope model SZX10 (Olympus, Tokyo, Japan) with a CCD camera (PD21, Olympus, Tokyo, Japan). Scanning electron microscopic (SEM) images were taken using an electron microscope (model TM1000, Hitachi, Tokyo, Japan).

Calculation of Eye Pigmentation Score—The eye images of adult flies were obtained. To quantitatively evaluate the degree of eye degeneration in the MJDtr-Q78 flies, the area of remaining normal pigment in their eyes were measured using the National Institutes of Health ImageJ software as follows: 1) extraction of the green color to produce grayscale images and determination of the area of compound eye as the region of interest (Fig. 2, *Q* and *R*); 2) smoothing of the images by Gaussian blur (Fig. 2*S*), production of binary images, and adjustment of the threshold of the binary images to determine the area of remaining normal pigment in the eyes (Fig. 2*T*); and 3) calculation of the mean area of remaining normal pigment within the region of interest. For the TDP-43 flies, the region of interest was determined in the anterior half of the eye to avoid the necrotic tissues appeared in the posterior half because the necrotic tissues could be misjudged as normal pigment. More than four eyes were analyzed in each experiment.

Calculation of the Number of Interommatidial Bristles—The SEM images of adult fly eyes were obtained. The number of interommatidial bristles within a 150-μm^2 area in the eye was counted (23). Seven eyes were analyzed in each genotype.

Calculation of Eye Size—The light microscopic images of adult fly eyes were obtained. The eye size was measured using ImageJ software (24). Ten eyes were analyzed in each genotype.

Immunohistochemistry—Eye discs were dissected from third instar larvae, fixed with 4% paraformaldehyde, and then immunostained with a rat monoclonal anti-HA antibody (clone 3F10, Roche Applied Science), a rabbit polyclonal anti-Ref(2)P/p62 protein antibody (22), or a mouse monoclonal anti-elav antibody (clone 9F8A9, Developmental Studies Hybridoma Bank, Iowa City, IA) at 1:200 dilution as the primary antibody. As the secondary antibody, an Alexa 568-conjugated anti-rat antibody, an Alexa 488-conjugated anti-rabbit antibody, or an Alexa 488-conjugated anti-mouse antibody was used at 1:1000 dilution. Nuclei were stained using DAPI (Bio-Rad) after the secondary antibody staining. An Alexa 647-conjugated wheat germ agglutinin (Molecular Probes, Inc., Eugene, OR) staining to define the nuclear membrane was performed after DAPI staining at 1:500 dilution. Images were then taken by confocal laser-scanning microscopy (FV1000, Olympus, Tokyo, Japan).

[3] N. Fujikake, N. Kimura, Y. Saitoh, S. Nagano, Y. Hatanaka, T. Ishiguro, T. Takeuchi, M. Suzuki, H. A. Popiel, E. N. Minakawa, M. Ueyama, G. Matsumoto, A. Yokoseki, N. Nukina, T. Araki, O. Onodera, K. Wada, and Y. Nagai, submitted for publication.

The number of MJDtr-Q78 protein aggregates in the eye discs was quantitatively measured using the FV10-ASW 2.0 Viewer software (Olympus, Tokyo, Japan), as follows: 1) selection of photoreceptor neurons within the 13 developing ommatidia in row 2 and row 3 at the posterior tip of the eye discs, by anti-elav staining (Fig. 4, *E* and *F*), because these ommatidia are in approximately the same developing stage and can be easily identified; 2) counting of the number of MJDtr-Q78 protein aggregates localized in either the cytoplasm or the nucleus, judged by whether they merge with the nuclei stained with DAPI or not (Fig. 4, *G* and *H*). More than five eye discs were analyzed in each experiment.

Western Blot Analysis—Five heads of adult flies or 20 eye discs of larvae were lysed in 100 μl of SDS sample buffer using a pestle, sonicated, boiled for 5 min, and centrifuged at 10,000 × *g* for 3 min at 25 °C. The supernatants were run on a 5–20% gradient polyacrylamide gel (Wako, Osaka, Japan) and then transferred onto an Immun-Blot PVDF membrane (Bio-Rad). The membrane was blocked with 5% skim milk in PBS containing 0.1% Tween 20 for 30 min at room temperature and then incubated overnight with a rat monoclonal anti-HA antibody (clone 3F10, Roche Applied Science), a rabbit polyclonal anti-Ref(2)P/p62 antibody (22), or a mouse monoclonal anti-actin antibody (clone AC-40, Sigma-Aldrich) at 1:1000 dilution as primary antibody. After overnight incubation, the membranes were incubated with HRP-conjugated secondary antibodies. Membranes were then treated with SuperSignal West Dura chemiluminescent substrate (Thermo Fisher Scientific), and images were taken by the LAS-4000 imaging system (Fujifilm, Tokyo, Japan). Quantification of each signal was performed using the MultiGauge software (Fujifilm).

SDS-Agarose Gel Electrophoresis (SDS-AGE)—SDS-AGE was performed according to the previous reports (25–27). Briefly, adult fly head lysates were run on a 1.5% agarose, 0.1% SDS gel and then transferred onto a nitrocellulose membrane (Schleicher & Schuell BioScience). Blocking with skim milk, reaction with the primary or secondary antibody, and detection were done with the same protocols as Western blot analysis.

Gene Switch Protocol—RU486 (mifepristone, Sigma-Aldrich) was dissolved in 100% ethanol, further diluted in water, and then mixed with Instant *Drosophila* medium at a final concentration of 10 μg/ml (Carolina Biological Supply Company, Burlington, NC). For RU486 treatment, flies were in RU486-containing medium from the larval stage until adulthood.

Statistical Analyses—For comparisons between two groups, statistical differences were analyzed by Student's *t* test. Data are presented as the mean ± S.E. A p value of <0.05 was considered to indicate a statistically significant difference between groups.

RESULTS

p62 Co-localizes with Cytoplasmic PolyQ Protein Aggregates—To evaluate whether p62 affects the polyQ protein *in vivo*, we used the MJDtr-Q78S transgenic fly line, which expresses a truncated form of the mutant MJD protein with an expanded Gln-78 repeat (MJDtr-Q78). As a control, we used the MJDtr-Q27 transgenic fly line, which expresses a truncated form of the MJD protein with a normal-length Gln-27 repeat (MJDtr-Q27). The MJDtr-Q78S flies showed severe compound eye degeneration when the MJDtr-Q78 protein was selectively expressed in the eye by the *gmr-GAL4* driver, as revealed by light microscopic analyses (18) (Fig. 1*B*). On the contrary, the MJDtr-Q27 flies did not show any eye degenerative phenotypes (Fig. 1*A*). In these MJDtr-Q78S flies, the MJDtr-Q78 protein was found to accumulate as aggregates in both the cytoplasm and nucleus, although nuclear aggregates were more abundant than cytoplasmic aggregates (Fig. 1, *I* and *J*). To evaluate the relationship between p62 and the MJDtr-Q78 protein, we performed immunohistochemical analyses of larval eye discs. In the MJDtr-Q27 flies, p62 was predominantly present in the cytoplasm (Fig. 1, *C–H*), and punctate dotlike structures were also observed, which are known as "p62 bodies" (28) (Fig. 1*F*, *open arrows*). On the other hand, in the MJDtr-Q78S flies, p62 co-localized with cytoplasmic MJDtr-Q78 protein aggregates but not with nuclear aggregates (Fig. 1, *I–N*), although most MJDtr-Q78 protein aggregates were present in the nucleus. Wheat germ agglutinin staining to define the nuclear membrane revealed that p62-positive MJDtr-Q78 protein aggregates are present in the cytoplasm, and p62-negative MJDtr-Q78 protein aggregates are present in the nucleus (Fig. 1, *O–Q*). The size of p62-positive MJDtr-Q78 protein aggregates was much larger than that of the p62 bodies seen in the control flies, indicating that these p62-positive MJDtr-Q78 protein aggregates are different from the p62 bodies (Fig. 1, *F* and *L*). These results suggest that p62 is associated with the MJDtr-Q78 protein, especially with its cytoplasmic aggregates.

Loss of p62 Function Causes Exacerbation of Eye Degeneration in PolyQ Disease Model Flies—To evaluate the role of p62 in the pathomechanisms of the polyQ disease model flies, we examined the effect of the loss of p62 function on eye degeneration in two different MJDtr-Q78 fly lines: MJDtr-Q78S and MJDtr-Q78W flies. The latter flies express a lower expression level of the MJDtr-Q78 protein and show milder eye degeneration than the MJDtr-Q78S flies (Fig. 2, *A*, *B*, *E*, and *I*). We used a transgenic RNAi fly line that expresses an inverted repeat RNA (IR) of *ref(2)P*, the *Drosophila* ortholog of the *p62* gene, and two different mutant fly lines of *p62*: *ref(2)P*^{od2}, bearing a deletion of the Phox and Bem1p (PB1) domain, and *ref(2)P*^{od3}, bearing a deletion of the ubiquitin-associated domain (22). We confirmed the efficient knockdown of p62 protein expression when p62-IR is expressed throughout the whole fly body by the *tub-GAL4* driver (Fig. 2, *C* and *D*). When we crossed the MJDtr-Q78S flies with the p62-IR flies or *p62* mutant flies, we found that *p62* knockdown or *p62* mutations significantly aggravate the compound eye degeneration of the MJDtr-Q78S flies, resulting in more severe depigmentation and the appearance of necrotic tissue (Fig. 2, *E–H*). Knockdown of *p62* caused more severe eye degeneration than *p62* mutations, probably because *p62* mutant flies also possess a wild-type *p62* allele in *trans* to the mutant allele. Next, we examined the effect of loss of p62 function in the MJDtr-Q78W fly line. Knockdown of *p62* or *p62* mutations caused the exacerbation of eye depigmentation (Fig. 2, *I–L*), suggesting a protective role of p62 against polyQ-induced eye degeneration. Upon quantification of the eye pigmentation by imaging analyses (Fig. 2, *Q–T*), the exacerbation of eye depigmentation by *p62* knockdown or *p62* mutations was statistically significant (Fig. 2*U*). The exacerbation by loss of

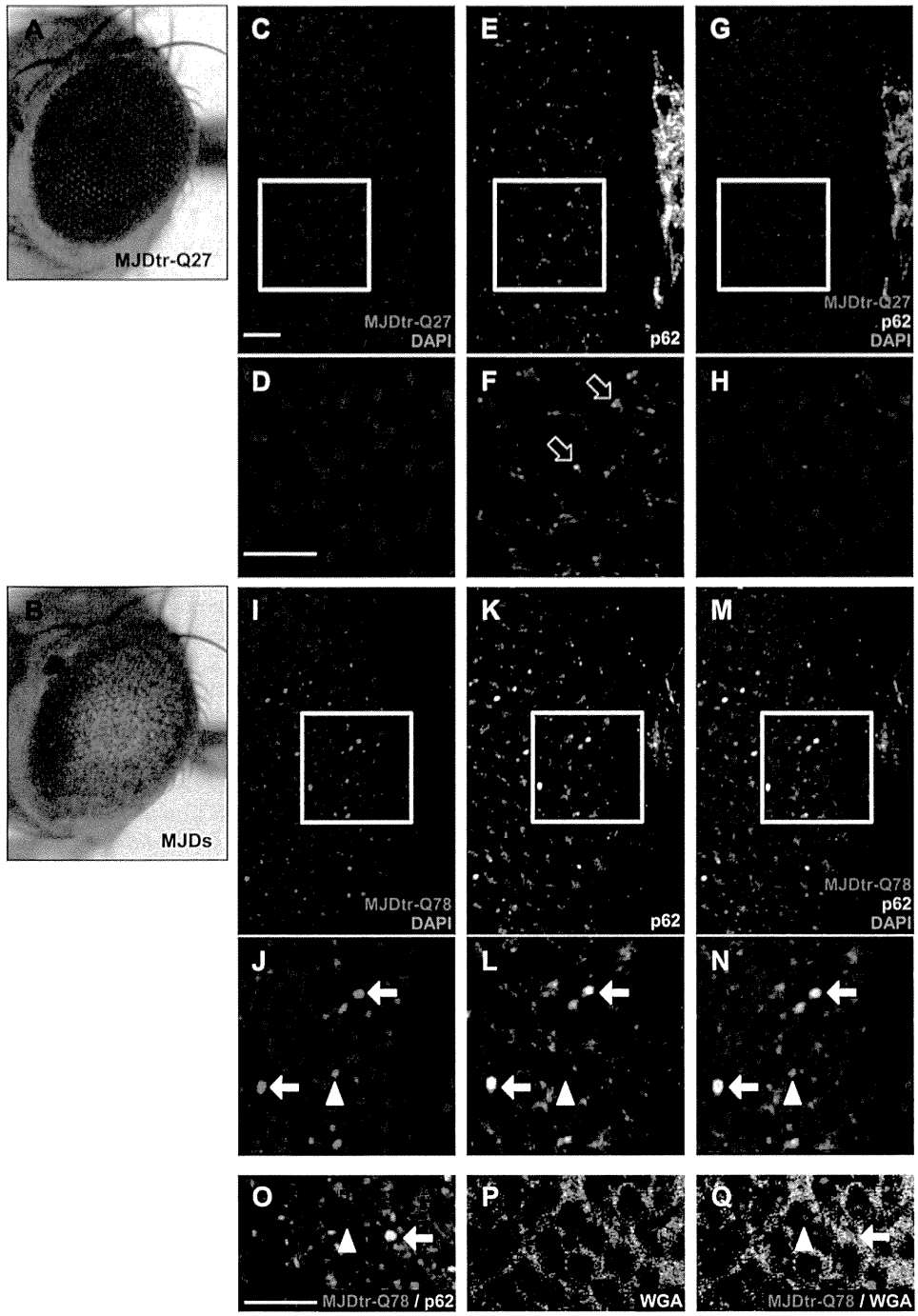

FIGURE 1. **p62 co-localizes with cytoplasmic aggregates of the MJDtr-Q78 protein.** *A* and *B*, light microscopic images of the external compound eyes of the control 1-day-old adult MJDtr-Q27 flies (*A*) and MJDtr-Q78S flies (*MJDs*) (*B*). *C–N*, confocal microscopic images of the larval eye discs of the control MJDtr-Q27 flies (*C–H*) and MJDtr-Q78S flies (*I–Q*), stained with an anti-HA antibody to detect the MJDtr-Q27 or MJDtr-Q78 protein (*red*), an anti-Ref(2)P/p62 antibody (*white* in *E*, *F*, *K*, and *L* and *green* in *G*, *H*, *M*, *N*, and *O*), DAPI for nuclear staining (*blue*), and wheat germ agglutinin to define the nuclear membrane (*white* in *P* and *green* in *Q*). *D*, *F*, *H*, *J*, *L*, and *N*, high magnification images of the indicated areas of *C*, *E*, *G*, *I*, *K*, and *M*, respectively. The *white arrows* and *arrowheads* indicate cytoplasmic and nuclear MJDtr-Q78 protein aggregates, respectively, and the *open arrows* indicate punctate dotlike structures of p62. *Bars*, 10 μm. Fly genotypes were as follows: *gmr-GAL4/+;;UAS-MJDtr-Q27/+* (*A* and *C–H*) and *gmr-GAL4/+;UAS-MJDtr-Q78S/+* (*B* and *I–Q*).

p62 function became even more evident upon the age-related progression of eye degeneration (Fig. 3). We confirmed that either *p62* knockdown or *p62* mutation does not cause any deleterious effects on the eyes of the flies expressing the MJDtr-Q27 protein (Fig. 2, *M–P* and *V*) or expressing the GAL4 protein alone (data not shown), excluding the possibility that the exacerbation of eye degeneration could be a simple additive effect. Furthermore, to exclude the possibility that p62 generally affects any degeneration regardless of the cause, we examined the effect of *p62* knockdown on the flies expressing Grim, which causes eye degeneration by apoptosis (Fig. 2*W*). We found that eye degeneration in the *grim* flies is not affected by *p62* knockdown (Fig. 2, *W–Y*), suggesting that the protective role of p62 is specific to polyQ protein toxicity.

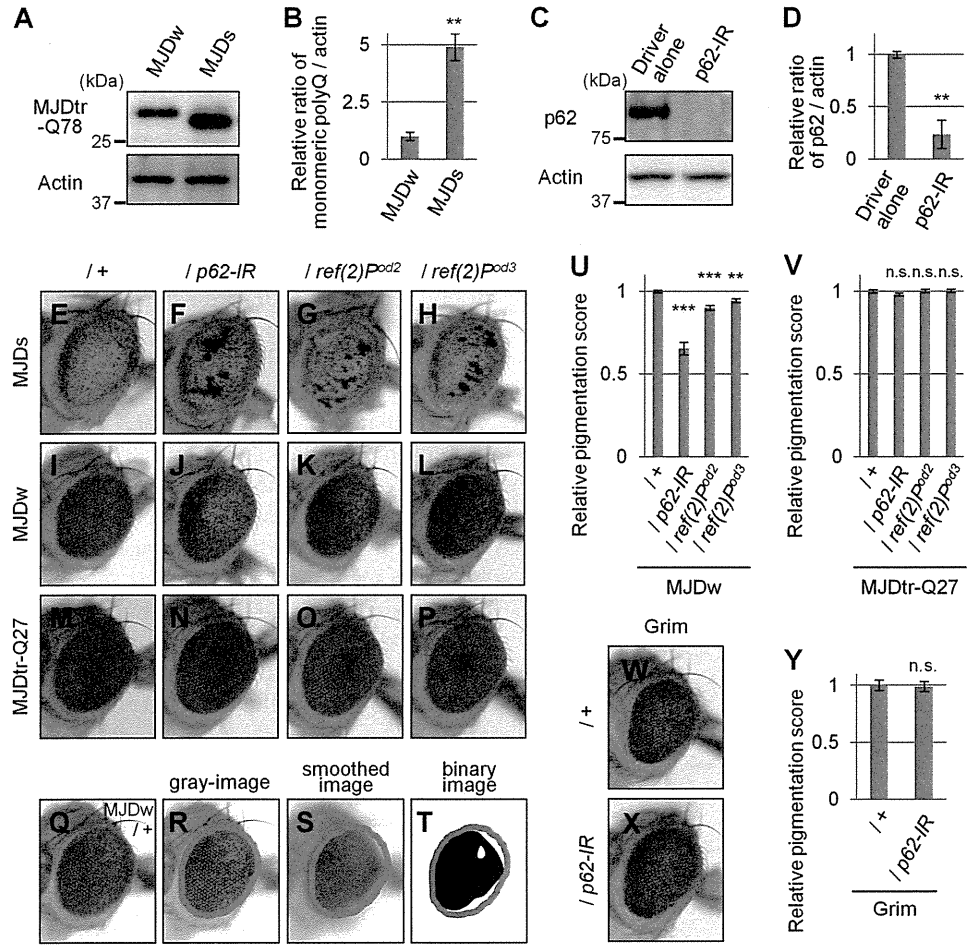

FIGURE 2. **Loss of p62 function causes exacerbation of eye degeneration in MJDtr-Q78 flies.** *A* and *B*, Western blot analysis of the monomeric MJDtr-Q78 protein in larval eye disc lysates of the MJDtr-Q78S flies (*MJDs*) and the MJDtr-Q78W (*MJDw*) flies expressing the MJDtr-Q78 protein under the *gmr-GAL4* driver, using an anti-HA antibody to detect the MJDtr-Q78 protein. The expression level of actin was used as a protein-loading control. The graph shows the relative ratio of the MJDtr-Q78 protein to actin. The relative amount of each protein was measured by densitometric analysis of the bands in *A*. Data are presented as the mean ± S.E. (**, $p < 0.01$, *versus* the MJDw flies) ($n = 3$). Fly genotypes were *gmr-GAL4/+;;UAS-MJDtr-Q78W/+* and *gmr-GAL4/+;UAS-MJDtr-Q78S/+*. *C* and *D*, knockdown efficiency of RNAi-mediated knockdown of *ref(2)P*, the *Drosophila* ortholog of the *p62* gene. The p62 protein in lysates prepared from adult fly heads expressing an IR targeted to *ref(2)P/p62* under the *tub-GAL4* driver was detected with the anti-Ref(2)P/p62 antibody by Western blot analysis. The expression level of actin was used as a protein-loading control. The graph shows the relative ratio of p62 protein to actin. The relative amount of each protein was measured by densitometric analyses of the bands in *C*. Data are presented as the mean ± S.E. (**, $p < 0.01$, *versus* the control flies expressing the GAL4 protein alone) ($n = 3$). Fly genotypes were *tub-GAL4/+* and *UAS-p62-IR/+;tub-GAL4/+*. *E–P*, light microscopic images of the external compound eyes of 1-day-old adult flies of two different MJDtr-Q78 fly lines, MJDtr-Q78S flies (*E*, *MJDs*) and MJDtr-Q78W flies (*I*, *MJDw*), expressing p62-IR (*F* and *J*) or bearing *p62* mutations, namely, *ref(2)P^{od2}* (*G* and *K*) and *ref(2)P^{od3}* (*H* and *L*), and the control MJDtr-Q27 flies (*M–P*). Note that the *p62* mutant flies also possess a wild-type *p62* allelle in *trans* to the mutant allele. Fly genotypes were as follows: *gmr-GAL4/+;UAS-MJDtr-Q78S/+* (*E*); *gmr-GAL4/+;UAS-MJDtr-Q78S/UAS-p62-IR* (*F*); *gmr-GAL4/+;UAS-MJDtr-Q78S/ref(2)P^{od2}* (*G*); *gmr-GAL4/+;UAS-MJDtr-Q78S/ref(2)P^{od3}* (*H*); *gmr-GAL4/+;;UAS-MJDtr-Q78W/+* (*I*); *gmr-GAL4/+;UAS-p62-IR/+;UAS-MJDtr-Q78W/+* (*J*); *gmr-GAL4/+;ref(2)P^{od2}/+;UAS-MJDtr-Q78W/+* (*K*); *gmr-GAL4/+;ref(2)P$^{od3/+}$UAS-MJDtr-Q78W/+* (*L*); *gmr-GAL4/+;;UAS-MJDtr-Q27/+* (*M*); *gmr-GAL4/+;UAS-p62-IR/+;UAS-MJDtr-Q27/+* (*N*); *gmr-GAL4/+;ref(2)P^{od2}/+;UAS-MJDtr-Q27/+* (*O*); and *gmr-GAL4/+;ref(2)P^{od3}/+;UAS-MJDtr-Q27/+* (*P*). *Q–T*, calculation of eye pigmentation score. Shown are light microscopic images of the external compound eye of an MJDtr-Q78W fly (*Q*; *MJDw*), the grayscale images extracted from *Q* (*R*), the smoothed image of *R* (*S*), and the binary image of *R* (*T*). *Red outlines* show the region of interest defined to evaluate the eye pigmentation. Note that the images shown here are representative images to explain this procedure clearly. The fly genotype used was *gmr-GAL4/+;;UAS-MJDtr-Q78W/+*. *U* and *V*, quantitative imaging analyses of eye pigmentation in the 1-day-old adult MJDtr-Q78W flies (*U*) or the control 1-day-old adult MJDtr-Q27 flies (*V*) expressing p62-IR alone or bearing *p62* mutations, namely *ref(2)P^{od2}* and *ref(2)P^{od3}*. More than four eye images were analyzed for each genotype. Data are presented as the mean ± S.E. (**, $p < 0.01$; ***, $p < 0.001$; *n.s.*, not significant, *versus* the MJDtr-Q78W flies in *U* and the MJDtr-Q27 flies in *V*, respectively). *W* and *X*, light microscopic images of the external compound eyes of 1-day-old adult flies expressing the Grim protein with or without *p62* knockdown. Fly genotypes were as follows: *gmr-GAL4/+;gmr-grim/+* (*W*) and *gmr-GAL4/+;gmr-grim/UAS-p62-IR* (*X*). *Y*, quantitative imaging analyses of eye pigmentation in the 1-day-old adult *grim* flies with or without expressing p62-IR. More than five eye images were analyzed for each genotype. Data are presented as the mean ± S.E. (*error bars*) (*n.s.*, not significant, *versus* the *grim* flies).

Loss of p62 Function Results in an Increase in Cytoplasmic PolyQ Protein Aggregates—To clarify the mechanisms underlying the protective role of p62 against polyQ protein toxicity, we evaluated the effect of *p62* knockdown on MJDtr-Q78 protein aggregates in the MJDtr-Q78S flies. Immunohistochemical analyses revealed that *p62* knockdown results in a robust increase in MJDtr-Q78 protein aggregates, especially those in the cytoplasm, compared with the control MJDtr-Q78S flies (Fig. 4, *A–D*). Upon quantification of the number of MJDtr-Q78 protein aggregates by imaging analyses (Fig. 4, *E–H*), we found that the increase in the number of MJDtr-Q78 protein aggregates by *p62* knockdown is statistically significant (Fig. 4, *I–K*), but the -fold change in the number of cytoplasmic aggregates was much higher than the -fold change in the number of

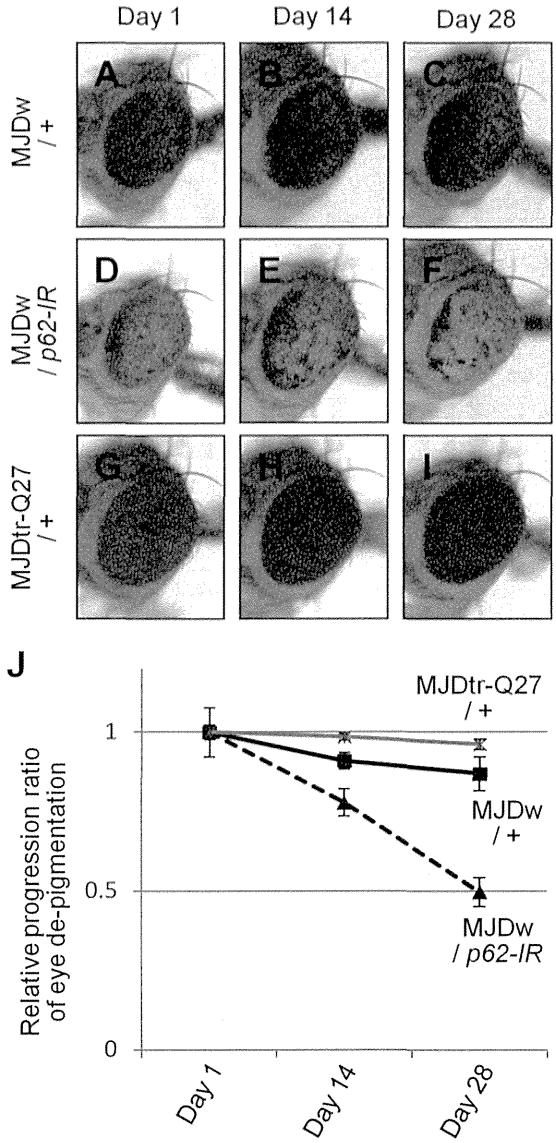

FIGURE 3. **The effect of *p62* knockdown on age-related progression of eye degeneration in the MJDtr-Q78W flies.** *A–F*, light microscopic images of the external compound eyes of 1-, 14-, and 28-day-old adult flies expressing the MJDtr-Q78 protein alone (*A–C*, MJDw/+) or co-expressing p62-IR (*D–F*, MJDw/*p62-IR*) and the control MJDtr-Q27 flies (*G–I*, MJDtr-Q27/+). *J*, relative progression ratio of eye depigmentation by performing quantitative imaging analyses of eye pigmentation in the MJDw flies with or without expressing p62-IR and the MJDtr-Q27 flies, respectively. More than five eye images were analyzed for each genotype. Data are presented as the mean ± S.E. (*error bars*). Fly genotypes were as follows: *gmr-GAL4/+;;UAS-MJDtr-Q78W/+* (*A–C*); *gmr-GAL4/+;UAS-p62-IR/+;UAS-MJDtr-Q78W/+* (*D–F*); and *gmr-GAL4/+;; UAS-MJDtr-Q27/+* (*G–I*).

nuclear aggregates (Fig. 4*L*). These results are consistent with the observation that p62 is predominantly localized in the cytoplasm and co-localizes with cytoplasmic MJDtr-Q78 protein aggregates (Fig. 1). These results suggest that the exacerbation of eye degeneration by *p62* knockdown in the MJDtr-Q78S flies is accompanied by the enhanced accumulation of cytoplasmic MJDtr-Q78 protein aggregates.

Loss of Autophagic Function Causes the Exacerbation of Eye Degeneration Accompanied by the Enhanced Accumulation of Cytoplasmic PolyQ Protein Aggregates—To evaluate whether the intrinsic protein degradation systems are involved in the toxicity of the polyQ protein, we examined the effect of both autophagic deficiency and UPS deficiency in the MJDtr-Q78 flies. For this purpose, we used the RNAi fly lines that express IRs of *Atg12* (autophagy-related gene 12), *alfy* (29), and *Prosβ2* (proteasome β2 subunit) and a mutant fly line of *Atg6* (*Atg6*^{00096}). We found that knockdown of the autophagy-related genes *Atg12* and *alfy* and the *Atg6* mutation result in significant exacerbation of eye degeneration in both the MJDtr-Q78S and MJDtr-Q78W flies (Fig. 5, *A–D*, *F–I*, and *P*). We also found that *Prosβ2* knockdown results in more severe exacerbation of the phenotypes of the MJDtr-Q78 flies, showing a lethal phenotype in the MJDtr-Q78S flies and more severe depigmentation in the MJDtr-Q78W flies (Fig. 5, *E*, *J*, and *P*). We confirmed that knockdown of *Atg12*, *alfy*, or *Prosβ2* or the *Atg6* mutation does not cause any deleterious effects on the eyes of the flies expressing the MJDtr-Q27 protein (Fig. 5, *K–O* and *Q*) or expressing the GAL4 protein alone (data not shown), excluding the possibility that the exacerbation of eye degeneration could be a simple additive effect.

We next evaluated the effects of autophagic or UPS function on MJDtr-Q78 protein aggregates. We found that *Atg12* knockdown significantly increases the number of MJDtr-Q78 protein aggregates, especially those in the cytoplasm, similarly to *p62* knockdown (Fig. 6, *A–D* and *G–J*). In contrast, *Prosβ2* knockdown resulted in a significant increase in MJDtr-Q78 protein aggregates only in the nucleus (Fig. 6, *E–J*). These results are consistent with the fact that protein degradation by autophagy takes place in the cytoplasm. These results imply that p62 plays a role similar to autophagy in the suppression of cytoplasmic polyQ protein aggregate formation.

Protective Role of p62 against PolyQ Protein Toxicity Is Dependent on Autophagy—To clarify whether the effects of *p62* on polyQ protein toxicity are dependent on autophagy or the UPS, we performed genetic analyses to examine the interaction between *p62* and genes involved in these two degradation systems. We crossed MJDtr-Q78W flies co-expressing p62-IR with flies expressing IRs targeted to either autophagy- or UPS-related genes. We found that additional knockdown of either *Atg12* or *alfy* in the MJDtr-Q78W flies together with *p62* knockdown does not show any additive effects on eye degeneration compared with that in the MJDtr-Q78W flies with *p62* knockdown alone (Fig. 7, *A–C* and *I*). On the contrary, additional knockdown of *Prosβ2* resulted in further exacerbation of eye degeneration in the MJDtr-Q78W flies with *p62* knockdown, as confirmed by quantitative imaging analyses (Fig. 7, *D* and *I*). We confirmed that knockdown of *Atg12*, *alfy*, or *Prosβ2* together with *p62* knockdown does not cause any deleterious effects on the eyes of the flies expressing the MJDtr-Q27 protein (Fig. 7, *E–H* and *J*) or expressing the GAL4 protein alone (data not shown), excluding the possibility that the exacerbation of eye degeneration could be a simple additive effect. These results suggest that *p62* plays a protective role against the toxicity of the MJDtr-Q78 protein via autophagy.

Loss of p62 Function Delays the Degradation of the PolyQ Protein in Vivo—To determine the role of p62 in degradation of the polyQ protein, we analyzed the MJDtr-Q78 protein expression level in the MJDtr-Q78S flies with or without *p62* knockdown. Western blot analyses of larval eye disc lysates of the

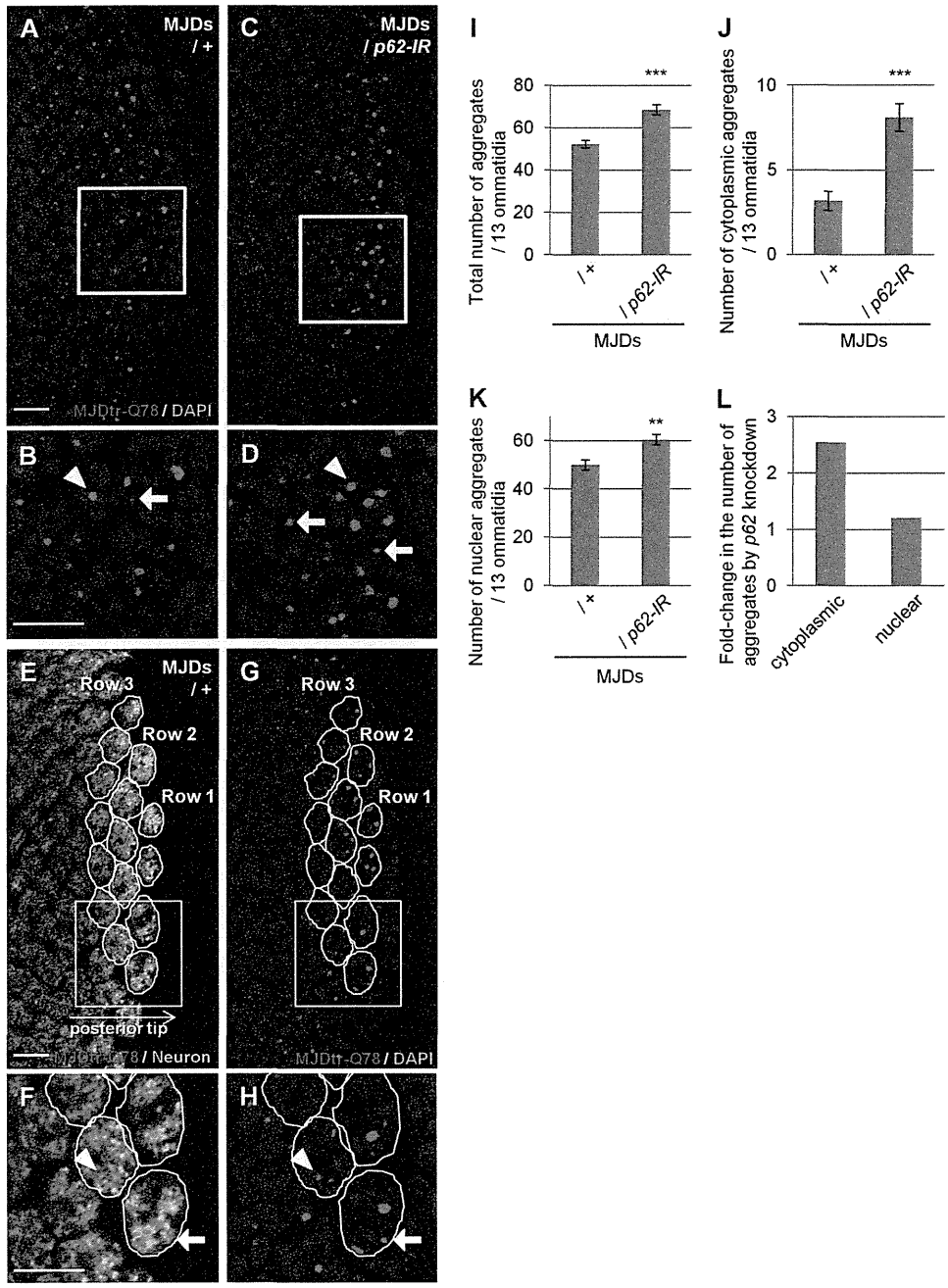

FIGURE 4. **Loss of p62 function results in an increase in cytoplasmic MJDtr-Q78 protein aggregates.** *A–D*, confocal microscopic images of the larval eye discs of flies expressing the MJDtr-Q78 protein alone (*A* and *B*, *MJDs*) or co-expressing p62-IR (*C* and *D*), stained with an anti-HA antibody to detect the MJDtr-Q78 protein (*red*) and DAPI for nuclear staining (*blue*). *B* and *D*, high magnification images of the indicated areas of *A* and *C*, respectively. The *arrows* and *arrowheads* indicate cytoplasmic and nuclear MJDtr-Q78 protein aggregates, respectively. *Bars*, 10 μm. Fly genotypes were as follows: *gmr-GAL4/+;UAS-MJDtr-Q78S/+* (*A* and *B*) and *gmr-GAL4/+;UAS-MJDtr-Q78S/UAS-p62-IR* (*C* and *D*). *E–H*, quantitative analyses of MJDtr-Q78 protein aggregates in the eye discs. Confocal microscopic images of an MJDtr-Q78S fly (MJDs) larval eye disc stained with an anti-HA antibody to detect the MJDtr-Q78 protein (*red*) and with an anti-elav antibody to detect the photoreceptor neurons (*E* and *F*, *green*). Nuclei were stained with DAPI (*G* and *H*, *blue*). Thirteen ommatidia in row 2 and row 3 at the posterior tip of the eye discs were selected (*yellow outlines*). *F* and *H*, high magnification images of the indicated areas of *E* and *G*, respectively. The MJDtr-Q78 protein aggregates were counted as either cytoplasmic aggregates (*arrow*) or nuclear aggregates (*arrowhead*), depending on whether they merged with the nucleus or not. The fly genotype used was *gmr-GAL4/+;UAS-MJDtr-Q78S/+*. *Bars*, 10 μm. *I–K*, the number of MJDtr-Q78 protein aggregates in the eye discs of MJDtr-Q78S flies with or without expression of p62-IR. The total numbers of MJDtr-Q78 protein aggregates (*I*), cytoplasmic aggregates (*J*), and nuclear aggregates (*K*) are presented. More than five eye discs were analyzed for both genotypes. Data are presented as the mean ± S.E. (*error bars*) (**, $p < 0.01$; ***, $p < 0.001$, *versus* the MJDtr-Q78S flies). *L*, the -fold change in the number of cytoplasmic or nuclear MJDtr-Q78 protein aggregates by *p62* knockdown.

MJDtr-Q78S flies constitutively expressing the MJDtr-Q78 protein by the *gmr-GAL4* driver revealed that knockdown of neither *p62* nor *Atg12* affects the MJDtr-Q78 protein expression level (Fig. 8, *A* and *B*). Because the MJDtr-Q78 protein expression level is dependent on the equilibrium between its expression and degradation, constitutive expression of the MJDtr-Q78 protein by the *gmr-GAL4* driver may make it difficult to detect alterations in MJDtr-Q78 protein turnover. Therefore, to evaluate MJDtr-Q78 protein turnover, we next used the inducible MJDtr-Q78S fly line, namely "ind-MJDtr-

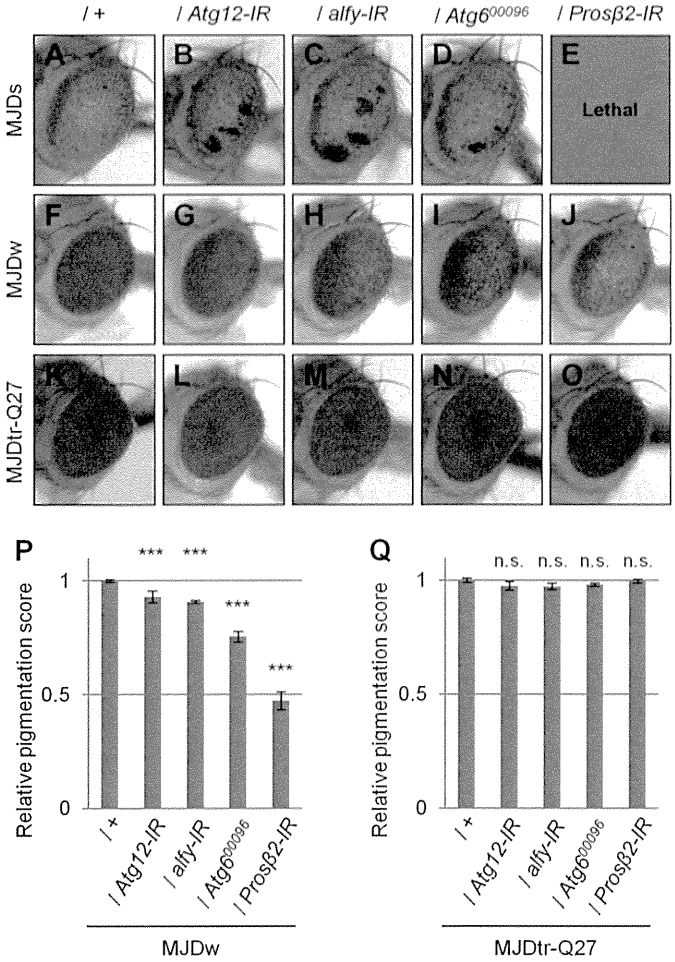

FIGURE 5. **Loss of autophagic or proteasomal function causes exacerbation of eye degeneration in MJDtr-Q78 flies.** *A–O*, light microscopic images of the external compound eyes of 1-day-old adult flies of two different MJDtr-Q78 fly lines, MJDtr-Q78S flies (*A*, *MJDs*) and MJDtr-Q78W flies (*F*, *MJDw*); MJDtr-Q78 flies co-expressing Atg12-IR (*B* and *G*), alfy-IR (*C* and *H*), or the proteasome β2 subunit (Prosβ2)-IR (*E* and *J*) or bearing an *Atg6* mutation (*Atg6*^{00096}) (*D* and *I*); and the control 1-day-old adult MJDtr-Q27 flies (*K–O*). Note that *Prosβ2* knockdown showed a lethal phenotype in the MJDtr-Q78S flies. Fly genotypes were as follows: *gmr-GAL4/+;UAS-MJDtr-Q78S/+* (*A*); *gmr-GAL4/+;UAS-MJDtr-Q78S/UAS-Atg12-IR* (*B*); *gmr-GAL4/+;UAS-MJDtr-Q78S/alfy-IR* (*C*); *gmr-GAL4/+;UAS-MJDtr-Q78S/+;Atg6*^{00096}*/+* (*D*); *gmr-GAL4/+;UAS-MJDtr-Q78S/+;Prosβ2-IR/+* (*E*); *gmr-GAL4/+;;UAS-MJDtr-Q78W/+* (*F*); *gmr-GAL4/+;UAS-Atg12-IR/+;UAS-MJDtr-Q78W/+* (*G*); *gmr-GAL4/+;UAS-alfy-IR/+;UAS-MJDtr-Q78W/+* (*H*); *gmr-GAL4/+;;UAS-MJDtr-Q78W/Atg6*^{00096} (*I*); *gmr-GAL4/+;;UAS-MJDtr-Q78W/Prosβ2-IR* (*J*); *gmr-GAL4/+;;UAS-MJDtr-Q27/+* (*K*); *gmr-GAL4/+;UAS-Atg12-IR/+;UAS-MJDtr-Q27/+* (*L*); *gmr-GAL4/+;alfy-IR/+;UAS-MJDtr-Q27/+* (*M*); *gmr-GAL4/+;;UAS-MJDtr-Q27/Atg6*^{00096} (*N*); and *gmr-GAL4/+;;UAS-MJDtr-Q27/Prosβ2-IR* (*O*). *P* and *Q*, quantitative imaging analyses of eye pigmentation in the 1-day-old adult MJDtr-Q78W flies (*P*) or the control 1-day-old adult MJDtr-Q27 flies (*Q*) expressing Atg12-IR, alfy-IR, or Prosβ2-IR or bearing an *Atg6* mutation. More than four eye images were analyzed for each genotype. Data are presented as the mean ± S.E. (*error bars*) (***, $p < 0.001$; *n.s.*, not significant, *versus* the MJDtr-Q78W flies in *P* and *versus* the MJDtr-Q27 flies in *Q*, respectively).

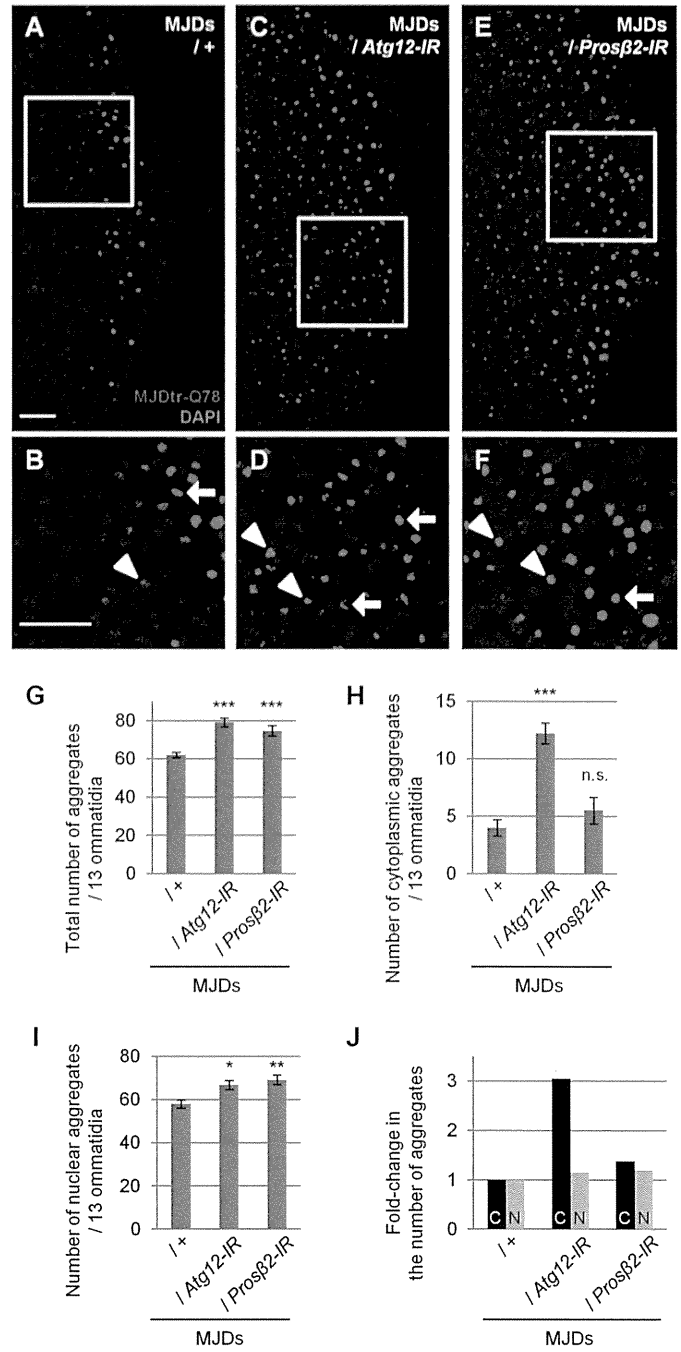

FIGURE 6. **Loss of autophagic function results in an increase in cytoplasmic MJDtr-Q78 protein aggregates.** *A–F*, confocal microscopic images of larval eye discs of flies expressing the MJDtr-Q78S protein alone (*A* and *B*, *MJDs*) or co-expressing either Atg12-IR (*C* and *D*) or the proteasome β2 subunit (*Prosβ2*)-IR (*E* and *F*), stained with an anti-HA antibody to detect the MJDtr-Q78 protein (*red*) and DAPI for nuclear staining (*blue*). *B*, *D*, and *F*, high magnification images of the indicated areas of *A*, *C*, and *E*, respectively. The *arrows* and *arrowheads* indicate cytoplasmic and nuclear MJDtr-Q78 protein aggregates, respectively. *Bars*, 10 μm. Fly genotypes used were as follows: *gmr-GAL4/+;UAS-MJDtr-Q78S/+* (*A* and *B*); *gmr-GAL4/+;UAS-MJDtr-Q78S/UAS-Atg12-IR* (*C* and *D*); and *gmr-GAL4/+;UAS-MJDtr-Q78S/+;Prosβ2-IR/+* (*E* and *F*). *G–I*, number of MJDtr-Q78 protein aggregates in the eye discs of MJDtr-Q78S flies with or without expression of Atg12-IR or Prosβ2-IR. The total numbers of MJDtr-Q78 protein aggregates (*G*), cytoplasmic aggregates (*H*), and nuclear aggregates (*I*) are presented. More than five eye discs were analyzed for each genotype. Data are presented as the mean ± S.E. (*error bars*) (*, $p < 0.05$; **, < 0.01; ***, $p < 0.001$; *n.s.*, not significant, *versus* the MJDtr-Q78S flies). *J*, -fold change in the number of cytoplasmic (*C*) or nuclear (*N*) MJDtr-Q78 protein aggregates by knockdown of *Atg12* or *Prosβ2*.

Q78S," which expresses the MJDtr-Q78 protein only in the presence of RU486 (mifepristone) under the control of the *gmr*-GeneSwitch (*gmr-GS*) driver (30). To validate this drug-inducible system *in vivo*, we evaluated the decay of the MJDtr-Q78 protein by Western blot analysis. RU486 was administered orally to ind-MJDtr-Q78 flies during the larval stage to induce MJDtr-Q78 protein expression. After emergence, RU486 was withdrawn to abolish MJDtr-Q78 protein expression. Western

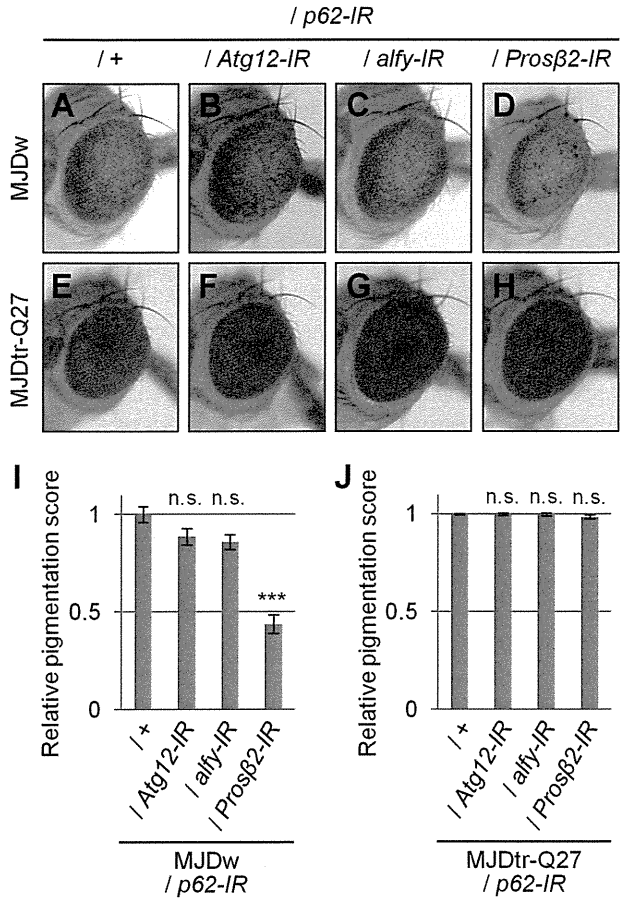

FIGURE 7. **Knockdown of autophagy-related genes in addition to *p62* knockdown does not cause additive exacerbation of eye degeneration in MJDtr-Q78W flies.** *A–H*, light microscopic images of the external compound eyes of 1-day-old adult MJDtr-Q78W (*MJDw*) flies with *p62* knockdown alone (*A*) or together with *Atg12* knockdown (*B*), *alfy* knockdown (*C*), or knockdown of *Prosβ2* (*D*) and the control 1-day-old adult MJDtr-Q27 flies (*E–H*). Fly genotypes used were as follows: *gmr-GAL4/+;UAS-p62-IR/+;UAS-MJDtr-Q78W/+* (*A*); *gmr-GAL4/+;UAS-p62-IR/UAS-Atg12-IR/+;UAS-MJDtr-Q78W/+* (*B*) *gmr-GAL4/+;UAS-p62-IR/UAS-alfy-IR;UAS-MJDtr-Q78W/+* (*C*); *gmr-GAL4/+;UAS-p62-IR/+;UAS-MJDtr-Q78W/Prosβ2-IR* (*D*); *gmr-GAL4/+;UAS-p62-IR/+;UAS-MJDtr-Q27/+* (*E*); *gmr-GAL4/+;UAS-p62-IR/UAS-Atg12-IR;UAS-MJDtr-Q27/+* (*F*); *gmr-GAL4/+;UAS-p62-IR/alfy-IR;UAS-MJDtr-Q27/+* (*G*); and *gmr-GAL4/+;UAS-p62-IR/+;UAS-MJDtr-Q27/Prosβ2-IR* (*H*). *I* and *J*, quantitative imaging analyses of eye pigmentation in the 1-day-old adult MJDtr-Q78W flies (*I*) or the control 1-day-old adult MJDtr-Q27 flies (*J*) with *p62* knockdown alone or together with *Atg12* knockdown, *alfy* knockdown, or *Prosβ2* knockdown. More than five eye images were analyzed for each genotype. Data are presented as the mean ± S.E. (*error bars*) (***, $p < 0.001$; *n.s.*, not significant, *versus* the MJDtr-Q78W flies with *p62* knockdown in *I* and *versus* the MJDtr-Q27 flies in *J*, respectively).

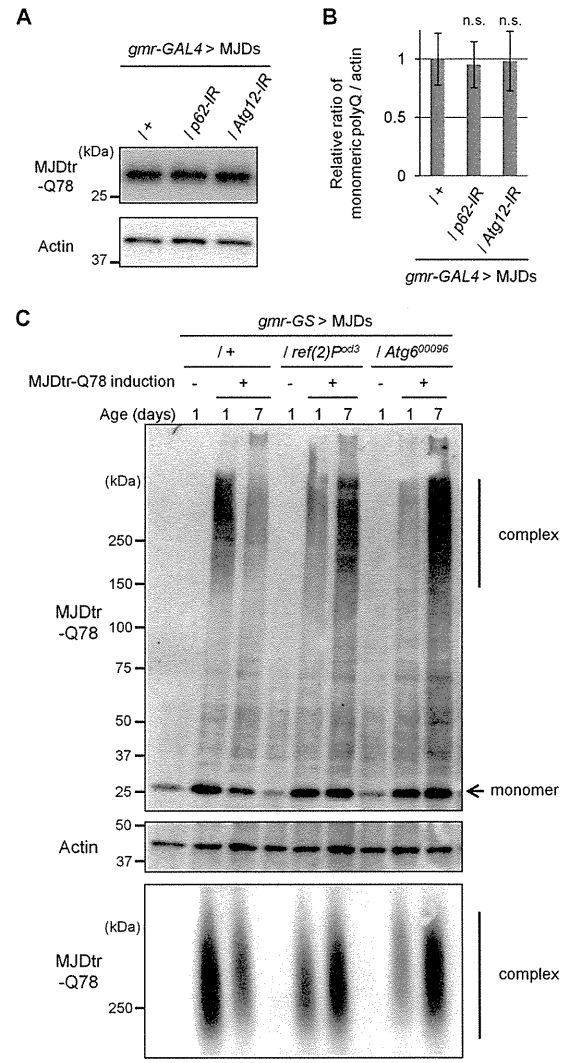

FIGURE 8. **Loss of p62 function delays the degradation of the MJDtr-Q78 protein *in vivo*.** *A* and *B*, Western blot analysis of the monomeric MJDtr-Q78 protein in larval eye disc lysates of the MJDtr-Q78S flies (*MJDs*) expressing the MJDtr-Q78 protein alone (+) or co-expressing either p62-IR or Atg12-IR under the *gmr-GAL4* driver, using an anti-HA antibody to detect the MJDtr-Q78 protein. The expression level of actin was used as a protein-loading control. The graph shows the ratio of the MJDtr-Q78 protein to actin. The relative amount of each protein was measured by densitometric analysis of the bands in *A*. Data are presented as the mean ± S.E. (*error bars*) (*n.s.*, not significant, *versus* the MJDtr-Q78S flies) ($n = 3–4$). Fly genotypes used were *gmr-GAL4/+;UAS-MJDtr-Q78S/+*, *gmr-GAL4/+;UAS-MJDtr-Q78S/UAS-p62-IR*, and *gmr-GAL4/+;UAS-MJDtr-Q78S/UAS-Atg12-IR*. *C*, Western blot analysis (*top* and *middle panels*) and SDS-AGE (*bottom panel*) of the MJDtr-Q78 protein in lysates prepared from 1-day-old and 7-day-old adult fly heads, expressing the MJDtr-Q78 protein alone (+) or bearing either the *p62* mutation (*ref(2)P^{od3}*) or *Atg6* mutation (*Atg6^{00096}*), under the *gmr*-GeneSwitch (*gmr-GS*) driver. MJDtr-Q78 protein expression was induced only during the larval stage by RU486 treatment (10 μg/ml) for the evaluation of MJDtr-Q78 protein turnover. In Western blot analysis, the monomeric MJDtr-Q78 protein (*monomer*) and its high molecular weight complexes (*complex*) were detected with an anti-HA antibody. The expression level of actin was used as a protein-loading control. The groups without MJDtr-Q78 protein induction (−) were evaluated for leak MJDtr-Q78 protein expression. In SDS-AGE, the high molecular weight complexes of the MJDtr-Q78 protein were detected with an anti-HA antibody. Fly genotypes used were *gmr-GS/+;UAS-MJDtr-Q78S/+*, *gmr-GS/+;UAS-MJDtr-Q78S/ref(2)P^{od3}*, and *gmr-GS/+;UAS-MJDtr-Q78S/+;Atg6^{00096}/+*.

blot analyses of lysates prepared from these adult fly heads demonstrated the gradual reduction of MJDtr-Q78 protein levels in the 7-day-old flies compared with the 1-day-old flies (Fig. 8*C*, +). These results suggest that both the monomeric MJDtr-Q78 protein and its high molecular weight complexes are efficiently degraded during the 6 days after emergence. The ind-MJDtr-Q78S flies without RU486 treatment showed slight leak expression of the MJDtr-Q78 protein. In this condition, we next analyzed the effects of p62 or autophagic deficiency on MJDtr-Q78 protein turnover. We crossed the ind-MJDtr-Q78S flies with *p62* or *Atg6* mutant flies, which are deficient in their functions independent of RU486 treatment. Western blot analyses showed that loss of p62 function clearly delays the degradation of both monomeric and high molecular weight complexes of the MJDtr-Q78 protein, similarly to loss of Atg6 function (Fig. 8*C*, *top* and *middle panels*). Surprisingly, the amounts of high molecular weight complexes of the MJDtr-Q78 protein were

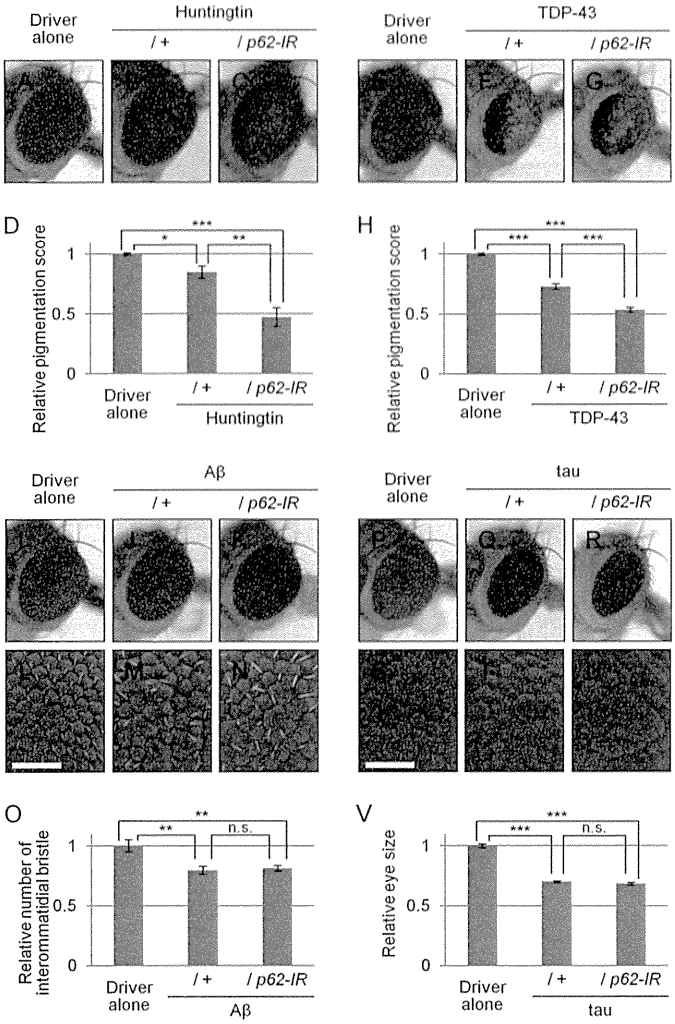

FIGURE 9. **Effects of loss of p62 function in various neurodegenerative disease model flies.** *A–C*, light microscopic images of the external compound eyes of 1-day-old adult flies expressing the mutant huntingtin protein with an expanded Gln-97 repeat with or without *p62* knockdown (*B* and *C*) and the control flies expressing the GAL4 protein alone (*A*). Fly genotypes used were as follows: *gmr-GAL4/+* (*A*); *gmr-GAL4/+;;UAS-Httex1p97QP/+* (*B*); *gmr-GAL4/+;UAS-p62-IR/+;UAS-Httex1p97QP/+* (*C*). *D*, quantitative imaging analyses of eye pigmentation in *A–C*. More than five eye images were analyzed for each genotype. Data are presented as the mean ± S.E. (*error bars*) (*, $p < 0.05$; **, $p < 0.01$; ***, $p < 0.001$, *versus* the control flies expressing the GAL4 protein alone). *E–G*, light microscopic images of the external compound eyes of 7-day-old adult flies expressing the human TDP-43 protein with or without *p62* knockdown (*F* and *G*), and the control flies expressing the GAL4 protein alone (*E*). Fly genotypes used were as follows: *gmr-GAL4/+* (*E*); *gmr-GAL4/+;UAS-*human *TDP-43/+* (*F*); and *gmr-GAL4/+;UAS-human TDP-43/UAS-p62-IR* (*G*). *H*, quantitative imaging analyses of eye pigmentation in *E–G*. More than five eye images were analyzed for each genotype. Data are presented as the mean ± S.E. (***, $p < 0.001$, *versus* the control flies expressing the GAL4 protein alone). *I–N*, light microscopic images (*I–K*) and SEM images (*L–N*) of the external compound eyes of 1-day-old adult flies expressing the mutant Aβ protein with or without *p62* knockdown (*J*, *K*, *M*, and *N*) and the control flies expressing the GAL4 protein alone (*I* and *L*). *Bars*, 50 μm. Fly genotypes used were as follows: *gmr-GAL4/+* (*I* and *L*); *gmr-GAL4/+;;UAS-Aβ arc2* (*J* and *M*); and *gmr-GAL4/+;UAS-p62-IR/+;UAS-Aβ arc2/+* (*K* and *N*). *O*, quantitative imaging analyses of the number of the interommatidial bristles in *L–N*. More than seven eye images were analyzed for each genotype. Data are presented as the mean ± S.E. (**, $p < 0.01$; n.s., not significant, *versus* the control flies expressing the GAL4 protein alone). *P–U*, light microscopic images (*P–R*) and SEM images (*S–U*) of the external compound eyes of 1-day-old adult flies expressing the mutant Tau protein with or without *p62* knockdown (*Q*, *R*, *T*, and *U*) and the control flies expressing the GAL4 protein alone (*P* and *S*). *Bars*, 50 μm. Fly genotypes used were as follows: *gmr-GAL4/+* (*P* and *S*); *gmr-GAL4/+;;UAS-R406W tau/+* (*Q* and *T*); and *gmr-GAL4/+;UAS-p62-IR/+; UAS-R406W tau/+* (*R* and *U*). *V*, quantitative imaging analyses of the eye size in *P–R*. More than 10 eye images were analyzed for each genotype. Data are presented as the mean ± S.E. (***, $p < 0.001$; *n.s.*, not significant, *versus* the control flies expressing the GAL4 protein alone).

rather increased by the loss of p62 or Atg6 function in the 7-day-old flies, implying that the monomeric MJDtr-Q78 protein that escaped from degradation assembles into oligomers during the 6 days. To further characterize these high molecular weight complexes of the MJDtr-Q78 protein, we performed the SDS-AGE blotting, allowing for the detection of SDS-soluble oligomeric species (25–27). The amounts of the slowly migrating SDS-soluble oligomeric species of the MJDtr-Q78 protein were clearly increased by the loss of p62 or Atg6 function in the 7-day-old flies, consistent with the results of Western blot analyses (Fig. 8*C*, *bottom panel*). These results suggest that loss of p62 function impairs autophagic degradation of the MJDtr-Q78 protein, especially its oligomeric species.

p62 Plays a Protective Role in Various Neurodegenerative Disease Model Flies—To evaluate whether the protective role of p62 is specific to MJDtr-Q78 flies, we examined the effects of *p62* knockdown in various neurodegenerative disease model flies. We used the Huntington disease model flies expressing a mutant huntingtin protein with an expanded Gln-97 repeat (19), the Alzheimer disease model flies expressing the mutant amyloid-β (Aβ) protein (20), the ALS model flies expressing the human TDP-43 protein, and the tauopathy model flies expressing the mutant Tau protein (21). In the huntingtin flies, *p62* knockdown resulted in significant exacerbation of eye degeneration, similarly to the MJDtr-Q78 flies (Fig. 9, *A–C*). Upon quantification of the eye pigmentation by imaging analyses in this model flies, the exacerbation of eye depigmentation by *p62* knockdown was statistically significant (Fig. 9*D*). In the TDP-43 flies, *p62* knockdown also resulted in significant exacerbation of eye degeneration (Fig. 9, *E–G*). Upon quantification of the eye pigmentation by imaging analyses in flies of this model, the exacerbation of eye depigmentation by *p62* knockdown was also statistically significant (Fig. 9*H*). On the contrary, the Aβ flies and the Tau flies did not show exacerbation of eye degeneration by *p62* knockdown, as revealed by both light microscopic and SEM analyses, respectively (Fig. 9, *I–N* and *P–U*). Upon quantification of the number of interommatidial bristles in the Aβ flies (Fig. 9, *L–N*) or the eye size in the Tau flies (Fig. 9, *P–R*), the exacerbation of eye degeneration by *p62* knockdown in both flies was not statistically significant (Fig. 9, *O* and *V*). These results suggest that p62 exerts protective effects not only against the polyQ protein but also against other proteins associated with neurodegenerative diseases.

DISCUSSION

In the present study, we provide evidence that p62 plays a protective role in the polyQ diseases *in vivo*. We demonstrated that the loss of p62 function causes a delay in the autophagic degradation of the polyQ protein, resulting in the enhanced accumulation of polyQ protein oligomers and cytoplasmic aggregates, and eventually leads to the exacerbation of the eye degeneration of polyQ disease model flies. We also genetically showed that these functions of p62 are dependent on autophagy. These results suggest that degradation of polyQ

protein oligomers is one of the important roles of p62 in protecting against polyQ protein toxicity.

Because p62 is delivered to the autophagosome by interaction with autophagosome membrane light chain 3 via the light chain 3-interacting region of p62 and recognizes ubiquitinated proteins via the ubiquitin-associated domain, p62 was suggested to be engaged in the selective autophagic degradation of ubiquitinated proteins, including the polyQ protein (13, 14). However, there have been substantial controversies regarding the role of p62 in polyQ cell culture models; one study reported that p62 depletion accelerates polyQ-induced cytotoxicity and it is rescued by p62 overexpression (28), whereas another study reported that p62 overexpression accelerates polyQ-induced cytotoxicity (31). In addition, some studies reported that p62 depletion does not affect the formation of polyQ protein aggregates (31–33). In this study, using polyQ disease model flies, we demonstrated that p62 depletion delays the autophagic degradation of the polyQ protein, including its oligomeric species, not merely its monomer. Our results are consistent with a recent report that depletion of p62 induces the accumulation of polyQ proteins in spinobulbar muscular atrophy model mice (34). These results suggest that p62-mediated autophagic degradation of the polyQ protein contributes to the protective effects of p62 against polyQ protein toxicity.

Our study clearly indicates the tight correlation between the amount of polyQ protein oligomers and the degree of neurodegeneration upon the loss of p62 function. Although several studies reported that the amount of polyQ protein inclusions does not correlate with neurodegeneration or that these inclusions are even protective, oligomeric species of misfolded polyQ proteins have been suggested as the principal culprit of neurodegeneration (6, 35). In other protein-misfolding neurodegenerative diseases, soluble oligomers composed of Aβ or α-synuclein have also been shown to exert cytotoxicity, suggesting the intrinsic toxicity of oligomeric structures, regardless of their primary amino acid sequences (36).

Although autophagy is known to act in the cytoplasm, our immunohistochemical analyses showed that p62 depletion also results in a modest increase in nuclear polyQ protein aggregates (Figs. 4 and 6). These results may be a secondary consequence of inefficient autophagic degradation of the polyQ protein, because Atg12 depletion also resulted in a similar consequence. A possible explanation for these results is that inefficient degradation of the polyQ protein in the cytoplasm may also result in an increase of polyQ proteins in the nucleus and their accumulation as nuclear aggregates.

In this study, we showed the protective role of p62 not only in the MJDtr-Q78 flies but also in other neurodegenerative disease flies, such as Huntington disease and TDP-43 proteinopathies (Fig. 9). These results are consistent with the previous reports that huntingtin and TDP-43 are degraded by autophagy (37–40). However, we could not detect the protective effect of p62 in the Aβ flies and the Tau flies. It is known that these Tau-expressing flies do not develop tangles consisting of misfolded Tau proteins (21). Moreover, the Tau protein is reported to be mainly degraded by the UPS rather than autophagy (41–43). In addition, the Aβ peptides are not ubiquitinated in the Alzheimer disease brain, and they are known to be degraded by endopeptidases, such as neprilysin and insulin-degrading enzyme (44, 45). Therefore, p62 could be involved in neurodegeneration in the polyQ and TDP-43 flies but not in the Aβ and Tau flies, although further studies are required to elucidate the mechanisms of the selectivity of p62.

Our study provides new evidence that p62 is involved in the autophagic degradation of the polyQ protein, including its oligomers, *in vivo*, indicating its therapeutic potential for the polyQ diseases. Considering the selectivity of p62 for ubiquitinated proteins, the next step toward developing a p62-based therapy for the polyQ diseases should be establishing a method for the efficient recognition and degradation of polyQ proteins and possibly other misfolded proteins. A recent study revealed that phosphorylation of p62 at serine 403 renders a higher affinity to the polyubiquitin chain, resulting in the efficient degradation of ubiquitinated proteins (33). Selective and efficient degradation of misfolded proteins, especially oligomers, by p62 is expected to be developed as a general therapeutic strategy against protein-misfolding neurodegenerative diseases in the future.

Acknowledgments—We thank Drs. E. N. Minakawa (National Center of Neurology and Psychiatry), T. Takeuchi (Kyoto University), M. Komatsu (Niigata University), and T. Yoshimori (Osaka University) for helpful discussions; Dr. D. Contamine (deceased; Université Versailles-St Quentin-en-Yvelines) for kindly providing the mutant fly lines ref(2)P^{od2} and ref(2)P^{od3} and the rabbit polyclonal anti-Ref(2)P/p62 antibody; and the Bloomington Drosophila Stock Center and the Vienna Drosophila Resource Center for the other fly lines. We also thank T. Okada for technical assistance.

REFERENCES

1. Gatchel, J. R., and Zoghbi, H. Y. (2005) Diseases of unstable repeat expansion: mechanisms and common principles. *Nat. Rev. Genet.* **6,** 743–755
2. Davies, S. W., Turmaine, M., Cozens, B. A., DiFiglia, M., Sharp, A. H., Ross, C. A., Scherzinger, E., Wanker, E. E., Mangiarini, L., and Bates, G. P. (1997) Formation of neuronal intranuclear inclusions underlies the neurological dysfunction in mice transgenic for the HD mutation. *Cell* **90,** 537–548
3. Scherzinger, E., Lurz, R., Turmaine, M., Mangiarini, L., Hollenbach, B., Hasenbank, R., Bates, G. P., Davies, S. W., Lehrach, H., and Wanker, E. E. (1997) Huntingtin-encoded polyglutamine expansions form amyloid-like protein aggregates *in vitro* and *in vivo*. *Cell* **90,** 549–558
4. Arrasate, M., Mitra, S., Schweitzer, E. S., Segal, M. R., and Finkbeiner, S. (2004) Inclusion body formation reduces levels of mutant huntingtin and the risk of neuronal death. *Nature* **431,** 805–810
5. Nagai, Y., Inui, T., Popiel, H. A., Fujikake, N., Hasegawa, K., Urade, Y., Goto, Y., Naiki, H., and Toda, T. (2007) A toxic monomeric conformer of the polyglutamine protein. *Nat. Struct. Mol. Biol.* **14,** 332–340
6. Takahashi, T., Kikuchi, S., Katada, S., Nagai, Y., Nishizawa, M., and Onodera, O. (2008) Soluble polyglutamine oligomers formed prior to inclusion body formation are cytotoxic. *Hum. Mol. Genet.* **17,** 345–356
7. Rubinsztein, D. C. (2006) The roles of intracellular protein-degradation pathways in neurodegeneration. *Nature* **443,** 780–786
8. Verhoef, L. G., Lindsten, K., Masucci, M. G., and Dantuma, N. P. (2002) Aggregate formation inhibits proteasomal degradation of polyglutamine proteins. *Hum. Mol. Genet.* **11,** 2689–2700
9. Holmberg, C. I., Staniszewski, K. E., Mensah, K. N., Matouschek, A., and Morimoto, R. I. (2004) Inefficient degradation of truncated polyglutamine proteins by the proteasome. *EMBO J.* **23,** 4307–4318
10. Venkatraman, P., Wetzel, R., Tanaka, M., Nukina, N., and Goldberg, A. L. (2004) Eukaryotic proteasomes cannot digest polyglutamine sequences and release them during degradation of polyglutamine-containing proteins. *Mol. Cell* **14,** 95–104

11. Ravikumar, B., Duden, R., and Rubinsztein, D. C. (2002) Aggregate-prone proteins with polyglutamine and polyalanine expansions are degraded by autophagy. *Hum. Mol. Genet.* **11,** 1107–1117
12. Johansen, T., and Lamark, T. (2011) Selective autophagy mediated by autophagic adapter proteins. *Autophagy* **7,** 279–296
13. Pankiv, S., Clausen, T. H., Lamark, T., Brech, A., Bruun, J. A., Outzen, H., Øvervatn, A., Bjørkøy, G., and Johansen, T. (2007) p62/SQSTM1 binds directly to Atg8/LC3 to facilitate degradation of ubiquitinated protein aggregates by autophagy. *J. Biol. Chem.* **282,** 24131–24145
14. Ichimura, Y., Kumanomidou, T., Sou, Y. S., Mizushima, T., Ezaki, J., Ueno, T., Kominami, E., Yamane, T., Tanaka, K., and Komatsu, M. (2008) Structural basis for sorting mechanism of p62 in selective autophagy. *J. Biol. Chem.* **283,** 22847–22857
15. Kuusisto, E., Salminen, A., and Alafuzoff, I. (2001) Ubiquitin-binding protein p62 is present in neuronal and glial inclusions in human tauopathies and synucleinopathies. *Neuroreport* **12,** 2085–2090
16. Kuusisto, E., Kauppinen, T., and Alafuzoff, I. (2008) Use of p62/SQSTM1 antibodies for neuropathological diagnosis. *Neuropathol. Appl. Neurobiol.* **34,** 169–180
17. Yamaguchi, M., Hirose, F., Inoue, Y. H., Shiraki, M., Hayashi, Y., Nishi, Y., and Matsukage, A. (1999) Ectopic expression of human p53 inhibits entry into S phase and induces apoptosis in the *Drosophila* eye imaginal disc. *Oncogene* **18,** 6767–6775
18. Warrick, J. M., Paulson, H. L., Gray-Board, G. L., Bui, Q. T., Fischbeck, K. H., Pittman, R. N., and Bonini, N. M. (1998) Expanded polyglutamine protein forms nuclear inclusions and causes neural degeneration in *Drosophila*. *Cell* **93,** 939–949
19. Steffan, J. S., Agrawal, N., Pallos, J., Rockabrand, E., Trotman, L. C., Slepko, N., Illes, K., Lukacsovich, T., Zhu, Y. Z., Cattaneo, E., Pandolfi, P. P., Thompson, L. M., and Marsh, J. L. (2004) SUMO modification of Huntingtin and Huntington's disease pathology. *Science* **304,** 100–104
20. Crowther, D. C., Kinghorn, K. J., Miranda, E., Page, R., Curry, J. A., Duthie, F. A., Gubb, D. C., and Lomas, D. A. (2005) Intraneuronal Aβ, non-amyloid aggregates and neurodegeneration in a *Drosophila* model of Alzheimer's disease. *Neuroscience* **132,** 123–135
21. Wittmann, C. W., Wszolek, M. F., Shulman, J. M., Salvaterra, P. M., Lewis, J., Hutton, M., and Feany, M. B. (2001) Tauopathy in *Drosophila*: neurodegeneration without neurofibrillary tangles. *Science* **293,** 711–714
22. Wyers, F., Petitjean, A. M., Dru, P., Gay, P., and Contamine, D. (1995) Localization of domains within the *Drosophila* Ref(2)P protein involved in the intracellular control of σ rhabdovirus multiplication. *J. Virol.* **69,** 4463–4470
23. Ueyama, M., Takemae, H., Ohmae, Y., Yoshida, H., Toyoda, H., Ueda, R., and Nishihara, S. (2008) Functional analysis of proteoglycan galactosyltransferase II RNA interference mutant flies. *J. Biol. Chem.* **283,** 6076–6084
24. Menzies, F. M., Garcia-Arencibia, M., Imarisio, S., O'Sullivan, N. C., Ricketts, T., Kent, B. A., Rao, M. V., Lam, W., Green-Thompson, Z. W., Nixon, R. A., Saksida, L. M., Bussey, T. J., O'Kane, C. J., and Rubinsztein, D. C. (2014) Calpain inhibition mediates autophagy-dependent protection against polyglutamine toxicity. *Cell Death Differ.* 10.1038/cdd.2014.151
25. Weiss, A., Klein, C., Woodman, B., Sathasivam, K., Bibel, M., Régulier, E., Bates, G. P., and Paganetti, P. (2008) Sensitive biochemical aggregate detection reveals aggregation onset before symptom development in cellular and murine models of Huntington's disease. *J. Neurochem.* **104,** 846–858
26. Legleiter, J., Mitchell, E., Lotz, G. P., Sapp, E., Ng, C., DiFiglia, M., Thompson, L. M., and Muchowski, P. J. (2010) Mutant huntingtin fragments form oligomers in a polyglutamine length-dependent manner *in vitro* and *in vivo*. *J. Biol. Chem.* **285,** 14777–14790
27. Sontag, E. M., Lotz, G. P., Yang, G., Sontag, C. J., Cummings, B. J., Glabe, C. G., Muchowski, P. J., and Thompson, L. M. (2012) Detection of mutant huntingtin aggregation conformers and modulation of SDS-soluble fibrillar oligomers by small molecules. *J. Huntingtons Dis.* **1,** 127–140
28. Bjørkøy, G., Lamark, T., Brech, A., Outzen, H., Perander, M., Overvatn, A., Stenmark, H., and Johansen, T. (2005) p62/SQSTM1 forms protein aggregates degraded by autophagy and has a protective effect on huntingtin-induced cell death. *J. Cell Biol.* **171,** 603–614
29. Filimonenko, M., Isakson, P., Finley, K. D., Anderson, M., Jeong, H., Melia, T. J., Bartlett, B. J., Myers, K. M., Birkeland, H. C., Lamark, T., Krainc, D., Brech, A., Stenmark, H., Simonsen, A., and Yamamoto, A. (2010) The selective macroautophagic degradation of aggregated proteins requires the PI3P-binding protein Alfy. *Mol. Cell* **38,** 265–279
30. Roman, G., and Davis, R. L. (2002) Conditional expression of UAS-transgenes in the adult eye with a new gene-switch vector system. *Genesis* **34,** 127–131
31. Korolchuk, V. I., Mansilla, A., Menzies, F. M., and Rubinsztein, D. C. (2009) Autophagy inhibition compromises degradation of ubiquitin-proteasome pathway substrates. *Mol. Cell* **33,** 517–527
32. Nagaoka, U., Kim, K., Jana, N. R., Doi, H., Maruyama, M., Mitsui, K., Oyama, F., and Nukina, N. (2004) Increased expression of p62 in expanded polyglutamine-expressing cells and its association with polyglutamine inclusions. *J. Neurochem.* **91,** 57–68
33. Matsumoto, G., Wada, K., Okuno, M., Kurosawa, M., and Nukina, N. (2011) Serine 403 phosphorylation of p62/SQSTM1 regulates selective autophagic clearance of ubiquitinated proteins. *Mol. Cell* **44,** 279–289
34. Doi, H., Adachi, H., Katsuno, M., Minamiyama, M., Matsumoto, S., Kondo, N., Miyazaki, Y., Iida, M., Tohnai, G., Qiang, Q., Tanaka, F., Yanagawa, T., Warabi, E., Ishii, T., and Sobue, G. (2013) p62/SQSTM1 differentially removes the toxic mutant androgen receptor via autophagy and inclusion formation in a spinal and bulbar muscular atrophy mouse model. *J. Neurosci.* **33,** 7710–7727
35. Schaffar, G., Breuer, P., Boteva, R., Behrends, C., Tzvetkov, N., Strippel, N., Sakahira, H., Siegers, K., Hayer-Hartl, M., and Hartl, F. U. (2004) Cellular toxicity of polyglutamine expansion proteins: mechanism of transcription factor deactivation. *Mol. Cell* **15,** 95–105
36. Kayed, R., Head, E., Thompson, J. L., McIntire, T. M., Milton, S. C., Cotman, C. W., and Glabe, C. G. (2003) Common structure of soluble amyloid oligomers implies common mechanism of pathogenesis. *Science* **300,** 486–489
37. Ravikumar, B., Vacher, C., Berger, Z., Davies, J. E., Luo, S., Oroz, L. G., Scaravilli, F., Easton, D. F., Duden, R., O'Kane, C. J., and Rubinsztein, D. C. (2004) Inhibition of mTOR induces autophagy and reduces toxicity of polyglutamine expansions in fly and mouse models of Huntington disease. *Nat. Genet.* **36,** 585–595
38. Martin, D. D., Ladha, S., Ehrnhoefer, D. E., and Hayden, M. R. (2014) Autophagy in Huntington disease and huntingtin in autophagy. *Trends Neurosci.* 10.1016/j.tins.2014.09.003
39. Brady, O. A., Meng, P., Zheng, Y., Mao, Y., and Hu, F. (2011) Regulation of TDP-43 aggregation by phosphorylation and p62/SQSTM1. *J. Neurochem.* **116,** 248–259
40. Scotter, E. L., Vance, C., Nishimura, A. L., Lee, Y. B., Chen, H. J., Urwin, H., Sardone, V., Mitchell, J. C., Rogelj, B., Rubinsztein, D. C., and Shaw, C. E. (2014) Differential roles of the ubiquitin proteasome system and autophagy in the clearance of soluble and aggregated TDP-43 species. *J. Cell Sci.* **127,** 1263–1278
41. Petrucelli, L., Dickson, D., Kehoe, K., Taylor, J., Snyder, H., Grover, A., De Lucia, M., McGowan, E., Lewis, J., Prihar, G., Kim, J., Dillmann, W. H., Browne, S. E., Hall, A., Voellmy, R., Tsuboi, Y., Dawson, T. M., Wolozin, B., Hardy, J., and Hutton, M. (2004) CHIP and Hsp70 regulate tau ubiquitination, degradation and aggregation. *Hum. Mol. Genet.* **13,** 703–714
42. Shimura, H., Schwartz, D., Gygi, S. P., and Kosik, K. S. (2004) CHIP-Hsc70 complex ubiquitinates phosphorylated Tau and enhances cell survival. *J. Biol. Chem.* **279,** 4869–4876
43. Lee, M. J., Lee, J. H., and Rubinsztein, D. C. (2013) Tau degradation: the ubiquitin-proteasome system versus the autophagy-lysosome system. *Prog. Neurobiol.* **105,** 49–59
44. Iwata, N., Tsubuki, S., Takaki, Y., Watanabe, K., Sekiguchi, M., Hosoki, E., Kawashima-Morishima, M., Lee, H. J., Hama, E., Sekine-Aizawa, Y., and Saido, T. C. (2000) Identification of the major Aβ_{1-42}-degrading catabolic pathway in brain parenchyma: suppression leads to biochemical and pathological deposition. *Nat. Med.* **6,** 143–150
45. Qiu, W. Q., Walsh, D. M., Ye, Z., Vekrellis, K., Zhang, J., Podlisny, M. B., Rosner, M. R., Safavi, A., Hersh, L. B., and Selkoe, D. J. (1998) Insulin-degrading enzyme regulates extracellular levels of amyloid β-protein by degradation. *J. Biol. Chem.* **273,** 32730–32738

jbc The Journal of Biological Chemistry

AFFINITY SITES

ASBMB American Society for Biochemistry and Molecular Biology

Molecular Bases of Disease:

p62 Plays a Protective Role in the Autophagic Degradation of Polyglutamine Protein Oligomers in Polyglutamine Disease Model Flies

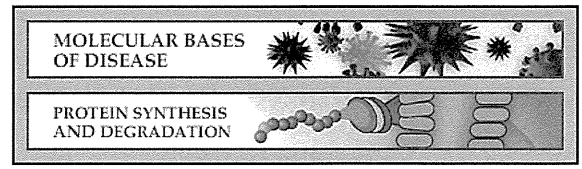

Yuji Saitoh, Nobuhiro Fujikake, Yuma Okamoto, H. Akiko Popiel, Yusuke Hatanaka, Morio Ueyama, Mari Suzuki, Sébastien Gaumer, Miho Murata, Keiji Wada and Yoshitaka Nagai

J. Biol. Chem. 2015, 290:1442-1453.
doi: 10.1074/jbc.M114.590281 originally published online December 5, 2014

Neurobiology of Disease 71 (2014) 1–13

Contents lists available at ScienceDirect

Neurobiology of Disease

journal homepage: www.elsevier.com/locate/ynbdi

VPS35 dysfunction impairs lysosomal degradation of α-synuclein and exacerbates neurotoxicity in a *Drosophila* model of Parkinson's disease

Emiko Miura [a,1], Takafumi Hasegawa [a,1,*], Masatoshi Konno [a,b,1], Mari Suzuki [b], Naoto Sugeno [a], Nobuhiro Fujikake [b], Sven Geisler [c], Mitsuaki Tabuchi [d], Ryuji Oshima [a], Akio Kikuchi [a], Toru Baba [a], Keiji Wada [b], Yoshitaka Nagai [b], Atsushi Takeda [a,e], Masashi Aoki [a]

[a] *Division of Neurology, Department of Neuroscience & Sensory Organs, Tohoku University Graduate School of Medicine, Sendai 980-8574, Japan*
[b] *Department of Degenerative Neurological Diseases, National Institute of Neuroscience, National Center of Neurology and Psychiatry (NCNP), Kodaira 187-8502, Japan*
[c] *Laboratory of Functional Neurogenetics, Department for Neurodegenerative Diseases, Hertie Institute for Clinical Brain Research, University of Tübingen, German Centre for Neurodegenerative Diseases (DZNE), 72076 Tübingen, Germany*
[d] *Laboratory of Applied Molecular Cell Biology, Faculty of Agriculture, Kagawa University, Kagawa 761-0795, Japan*
[e] *Department of Neurology, National Hospital Organization Sendai-Nishitaga Hospital, Sendai 982-8555, Japan*

ARTICLE INFO

Article history:
Received 3 May 2014
Revised 7 July 2014
Accepted 28 July 2014
Available online 6 August 2014

Keywords:
Parkinson's disease
VPS35
α-Synuclein
Retromer
Cathepsin D
Lysosome
Vesicular transport

ABSTRACT

Mutations in *vacuolar protein sorting 35* (*VPS35*) have been linked to familial Parkinson's disease (PD). VPS35, a component of the retromer, mediates the retrograde transport of cargo from the endosome to the trans-Golgi network. Here we showed that retromer depletion increases the lysosomal turnover of the mannose 6-phosphate receptor, thereby affecting the trafficking of cathepsin D (CTSD), a lysosome protease involved in α-synuclein (αSYN) degradation. VPS35 knockdown perturbed the maturation step of CTSD in parallel with the accumulation of αSYN in the lysosomes. Furthermore, we found that the knockdown of *Drosophila VPS35* not only induced the accumulation of the detergent-insoluble αSYN species in the brain but also exacerbated both locomotor impairments and mild compound eye disorganization and interommatidial bristle loss in flies expressing human αSYN. These findings indicate that the retromer may play a crucial role in αSYN degradation by modulating the maturation of CTSD and might thereby contribute to the pathogenesis of the disease.

Introduction

Parkinson's disease (PD), the second most common neurodegenerative disease, is clinically characterized by a progressive increase in movement disability, impaired balance, and a variety of nonmotor symptoms (Poewe and Mahlknecht, 2009). The pathological hallmark of PD is the loss of pigmented dopaminergic neurons in the substantia nigra pars compacta and the presence of Lewy bodies, which are composed primarily of α-synuclein (αSYN) fibrils (Spillantini et al., 1997). During the assembly of αSYN fibrils, various intermediate-state oligomers are formed, and these oligomers are suspected to be the main toxic species (Wales et al., 2013). The mechanisms underlying the selective neuronal loss in PD remain elusive; however, numerous etiopathogenic hypotheses have been proposed related to oxidative stress, endoplasmic reticulum stress, mitochondrial dysfunction, ubiquitin–proteasome dysfunction, and an impaired autophagy–lysosome pathway (Dehay et al., 2013; Hasegawa et al., 2006; Singleton et al., 2013; Springer and Kahle, 2011; Sugeno et al., 2008; Tofaris, 2012). Although more than 90% of PD cases occur sporadically, the identification of several genes linked to familial PD has offered great insight into the biochemical and molecular mechanisms of the disease. Recently, a missense mutation (p.D620N) in the *vacuolar protein sorting 35* (*VPS35*) gene was identified as the cause of an autosomal dominant form of PD (Vilarino-Guell et al., 2011; Zimprich et al., 2011). VPS35, a vital element of the retromer complex, mediates the retrograde

Abbreviations: Ab, antibody; AD, Alzheimer's disease; αSYN, α-synuclein; CTSD, cathepsin D; CI-MPR, cation-independent mannose 6-phosphate receptor; DMEM, Dulbecco's modified Eagle's medium; elav, embryonic lethal abnormal vision; FBS, fetal bovine serum; GMR, glass multiple reporter; HMW, high-molecular-weight; HRP, horseradish peroxidase; HSP, heat shock protein; LAMP, lysosome-associated membrane protein; M6P, mannose 6-phosphate; MTT, 3-(4,5-dimethylthiazo-2-yl)-2,5-diphenyltetrazolium bromide; NAB, N-aryl benzimidazole; Nedd4, neural precursor cell expressed developmentally down-regulated protein 4; PD, Parkinson's disease; PVDF, polyvinylidene difluoride; RFU, relative fluorescence unit; RIPA, radio-immunoprecipitation assay; RNAi, RNA interference; rp49, ribosomal protein 49; siRNA, small interfering RNA; SDS, sodium dodecyl sulfate; SNX, sorting nexin; TCA, trichloroacetic acid; Tg, transgenic; TGN, trans-Golgi network; UAS, upstream activating sequence; VPS35, vacuolar protein sorting 35; WASH, Wiskott–Aldrich syndrome protein and SCAR homolog; wt, wild-type.

* Corresponding author at: Division of Neurology, Department of Neuroscience & Sensory Organs, Tohoku University Graduate School of Medicine, 1-1, Seiryomachi, Aobaku, Sendai, Miyagi 980-8574, Japan. Fax: +81 22 717 7192.
E-mail address: thasegawa@med.tohoku.ac.jp (T. Hasegawa).
Available online on ScienceDirect (www.sciencedirect.com).
[1] These authors contributed equally to this study.

http://dx.doi.org/10.1016/j.nbd.2014.07.014
0969-9961/

transport of cargo from the endosome to the *trans*-Golgi network (TGN) (Seaman et al., 1997). Structurally, the retromer comprises two distinct subcomplexes: a cargo-recognition VPS26–VPS29–VPS35 heterotrimer and a membrane-targeting dimer of the sorting nexin (SNX1 and/or SNX2) (Hierro et al., 2007). One of the best-characterized types of cargo for the retromer is the cation-independent mannose 6-phosphate receptor (CI-MPR), which participates in the delivery of lysosomal enzymes, such as the aspartyl protease cathepsin D (CTSD), to lysosomes (Seaman, 2004). Upon arrival in the Golgi apparatus, newly synthesized lysosomal enzymes are specifically modified with mannose 6-phosphate (M6P) residues, which are recognized by the CI-MPR in the TGN. Under physiological conditions, newly synthesized CTSD binds CI-MPR in the TGN and is translocated into endosomes; the CTSD is then released for further transport to lysosomes. The retromer retrieves the unoccupied MPRs from endosomes and relocates them to the TGN, where they participate in further cycles of CTSD sorting. Because CTSD is the main lysosomal endopeptidase responsible for the degradation of long-lived proteins, including αSYN (Cullen et al., 2009; Sevlever et al., 2008), it is tempting to speculate that a VPS35 malfunction may decrease the active form of CTSD in lysosomes and thus lead to an abnormal αSYN accumulation.

To further clarify the pathophysiological roles of the retromer in αSYN catabolism, RNA interference (RNAi)-mediated silencing of *VPS35* was performed using cellular and *in vivo* human wild-type (wt) αSYN (*h[wt]-SNCA*)-expressing transgenic fly models. In this study, we found that interference with the retromer function resulted in the aberrant maturation of CTSD, which led to the accumulation of intracellular αSYN, mainly in the late endosome/lysosome compartments. Furthermore, we showed that the knockdown of *Drosophila melanogaster VPS35* (*dVPS35*) exacerbated the locomotor abnormalities and mild compound eye disorganization and interommatidial bristle loss in human αSYN transgenic (Tg) flies. Our study provides evidence that the retromer may play a critical role in αSYN catabolism and thus drive the pathogenic process in synucleinopathies.

Materials and methods

Cell culture and plasmid transfection

HEK293 cells were maintained in Dulbecco's modified Eagle's medium (DMEM) with high glucose (4500 mg/L; Life Technologies/GIBCO, Carlsbad, CA) supplemented with L-glutamine and 10% fetal bovine serum (FBS; Thermo Scientific/HyClone, Rockford, IL). Plasmids (5 μg DNA for 1×10^6 cells) were introduced into these cells using the NEPA21® square wave electroporator according to the manufacturer's protocol (NEPA Gene, Chiba, Japan). Electroporation parameters consisted of a poring pulse (115 V, 7.5 ms in length with 50 ms interval) and a transfer pulse (20 V, 50 ms in length with 50 ms interval). For the stable transfection of HA-tagged and untagged αSYN in HEK293 cells, transfected cells were maintained under selective pressure with 800 μg/ml of G418 (InvivoGen, San Diego, CA).

Plasmid construction and preparation

Human CTSD cDNA (NM_001909.4) was subcloned into a pCMV vector. The cDNA encoding h[wt]-SNCA (NM_000345.3) with a Kozak consensus sequence was introduced into pcDNA3.1 + and 2xHA pRc/CMV vectors (RIKEN Bioresource Center, Tsukuba, Japan). Human wt and mutant (D620N and P316S) VPS35 cDNAs (GenBank AF175265.1) were subcloned into a pcDNA6.2/N-V5 vector (Life Technologies). Plasmid DNAs were isolated and purified using the GenoPure Plasmid Maxi Kit (Roche, Indianapolis, IN). The fidelity and orientation of the expression constructs were confirmed by restriction digestion and direct nucleotide sequencing.

RNA interference

The following small interfering RNAs (siRNAs) were used to ablate the expression of human VPS35: *VPS35* siRNA#1, 5′-GCCUUCAGAGGAUGUUGUAUCUUUA-3′ and *VPS35* siRNA#2, 5′-GCAUGAGUUGUUAUGUGCUUAGUAA-3′ (Stealth™ siRNA duplex oligoribonucleotides, Life Technologies/Invitrogen). Scrambled control siRNA (sc-36869) was purchased from Santa Cruz Biotechnology (Santa Cruz, CA). HEK293 cells were transfected with the target-specific or control scrambled siRNA (2 μg siRNA for 1×10^6 cells) using a NEPA21 square wave electroporator according to the manufacturer's protocol. Electroporation parameters included a poring pulse (115 V, 7.5 ms in length with 50 ms intervals) and a transfer pulse (20 V, 50 ms in length with 50 ms intervals). Thirty-three hours after the gene silencing, the cells were harvested and subjected to further studies. To evaluate the degradation kinetics of αSYN by CTSD, human CTSD was expressed for 24 h in HEK293 cells stably expressing αSYN. The cells were then treated with cycloheximide (0.1 μg/μl, purchased from Sigma) for 24 h. Chloroquine diphosphate (Sigma; 50 μM for 5 h) was used to examine the role of lysosomal function on αSYN degradation.

Subcellular fractionation

Subcellular fractionation was performed according to methods described previously (Hasegawa et al., 2011). In brief, mechanically harvested cells (1×10^8) were resuspended in 2 ml ice-cold fractionation buffer (10 mM Tris/acetic acid pH 7.0 and 250 mM sucrose) and homogenized using 20 strokes in a 2-ml Dounce tissue grinder with a tight pestle (GPE, Bedfordshire, England). The homogenate was cleared by three successive centrifugation steps (500 ×*g* for 2 min, 1000 ×*g* for 2 min and 2000 ×*g* for 2 min). The supernatant was centrifuged at 4000 ×*g* for 2 min to pellet the plasma membrane and nuclei. The supernatant was then ultracentrifuged at 100,000 ×*g* (P50S2 swing rotor, Hitachi Koki Co., Ltd., Tokyo, Japan) for 2 min to pellet the mitochondria, endosomes, and lysosomes (fraction EL). Lysosomes were isolated from the fraction EL by a 10-min osmotic lysis using 5 times the pellet volume of distilled water. After another centrifugation step at 100,000 ×*g* for 2 min, the lysosomes remained in the supernatant, whereas the endosomes and mitochondria were in the pellet.

Protein extraction from culture medium

Protein in the medium was extracted using a trichloroacetic acid (TCA)/acetone precipitation (Hasegawa et al., 2011). In brief, the culture medium was cleared by three successive centrifugation steps (800 ×*g* for 5 min, 2000 ×*g* for 10 min, and 10,000 ×*g* for 20 min at 4 °C). The supernatant was transferred to a new tube, and an equal volume of ice-cold 20% TCA/acetone was added, followed by incubation at −20 °C for 3 h. After adding 3 volumes of acetone, the protein was allowed to precipitate overnight at −20 °C. The protein was pelleted by centrifugation at 5000 ×*g* for 60 min, dissolved in 8 M urea/5% SDS with sonication, and subjected to Western blotting.

Cathepsin D activity assay

The bioactivity of CTSD in cultured cells was measured by a fluorescence-based assay using MCA-GKPILFFRLK(DNP)-dR-NH_2 as a synthetic substrate (CTSD Activity Assay Kit; BioVision, Mountain View, CA). Fluorescence was measured at an excitation/emission = 328/460 nm using a Varioskan Flash microplate reader (Thermo Scientific, Asheville, NC). The specific enzymatic activity was calculated as the relative fluorescence unit divided by the total protein concentration (relative fluorescence unit; RFU/μg protein). Pooled data from 5 independent experiments were statistically analyzed using one-way ANOVA with a post-hoc Dunnett's test using GraphPad Prism version 6 for Mac OS X (GraphPad Software, CA).

Western immunoblot analysis

After preparing the cell lysates using radio-immunoprecipitation assay (RIPA) buffer (1% NP-40, 0.5% deoxycholate, 0.1% sodium dodecyl sulfate (SDS), 1 mM EDTA, 10 m M sodium pyrophosphate, 50 mM sodium fluoride, 1 mM sodium orthovanadate, 150 mM sodium chloride, 50 mM Tris–HCl (pH 8.0) plus 1× Cømplete protease inhibitor cocktail; Roche), the protein concentration was determined using a BCA protein assay kit (BioRad, Hercules, CA). The lysate (15 μg) was electrophoresed on SDS-PAGE gels and transferred onto polyvinylidene difluoride (PVDF) membranes using the Trans-Blot Turbo® transfer system (BioRad). For the detection of human αSYN in the fly brain, five dissected fly heads were homogenized in Triton lysis buffer (50 mM Tris–HCl (pH 7.4), 1% Triton X-100, 150 mM NaCl, 1 mM EDTA plus protease inhibitors) using a Biomasher II® tissue grinder (Nippi Inc., Tokyo, Japan). After centrifugation at 15,000 ×*g* for 20 min, the supernatant was collected as the Triton-soluble fraction. The remaining pellet was further dissolved into a 2× Laemmli buffer with sonication and was centrifuged at 15,000 ×*g* for 20 min. The supernatant was collected as the Triton-insoluble fraction. For improved detection of αSYN in fly brain, transferred PVDF membranes were soaked in 0.4% paraformaldehyde/PBS for 30 min prior to the blocking step (Lee and Kamitani, 2011). After blocking with 5% milk in Tris-buffered saline with 0.1% Tween 20, the membranes were incubated with the following antibodies (Abs): anti-VPS35 ([C3], C-term Ab, 1:2000; GeneTex, Irvine, CA), anti-CTSD (clone C-20, 1:2000; Santa Cruz), anti-CI-MPR (#5230-1, 1:20,000; Epitomics, Burlingame, CA), anti-VPS26 (ab23892, 1:4000; Abcam, Cambridge, UK), anti-VPS29 (H00051699-A01, 1:500; Abnova, Taipei, Taiwan), anti-α-tubulin (clone DM1A, 1:1000; Sigma, St. Louis, MO), anti-syn-1 (610787, 1:1000; BD Bioscience, San Jose, CA), anti-HA-tag (clone 6E2, 1:1000; CST, Danvers, MA), anti-V5-tag (R960-25, 1:1000; Invitrogen), anti-albumin (#4929, 1:4000; CST), anti-Rab5 (clone S-19, 1:2000; Santa Cruz), anti-LAMP-2 (clone H4B4, 1:1000; DSHB, Iowa City, IA) and anti-Hsp90 (SPA-846, 1:4000; Stressgen, Victoria, BC, Canada). Primary Abs were followed by incubation with HRP-conjugated secondary Abs (1:10000; Jackson ImmunoResearch Laboratories, West Grove, PA). Bands were visualized with Luminata Forte HRP Substrate (Millipore, Bedford, MA) and images were captured by an Omega Lum G™ image analyzer (Aplegen, Pleasanton, CA). Quantification of the band intensity was performed using Image J software (NIH, Bethesda, MD). Pooled data from four independent experiments were statistically analyzed by a one-way ANOVA or unpaired Student's *t*-test.

Coimmunoprecipitation

Coimmunoprecipitation was performed according to the method described previously (Hasegawa et al., 2010). In brief, 48 h post-transfection, HEK293 cells were lysed in TNE buffer containing 50 mM Tris–HCl (pH 7.4), 150 mM NaCl, 0.5% NP-40, 1 mM EDTA and 1× protease inhibitor cocktail (Roche). Lysate containing 500 μg of protein was immunoprecipitated with 3 μl of V5 Ab (Life Technologies/Invitrogen) overnight on a carousel at 4 °C. Immune complexes were allowed to bind to Protein A/G PLUS-Agarose (Santa Cruz) for 2 h at 4 °C. After washing 5 times with TNE buffer containing 0.1% NP-40, protein complexes were eluted with 2× non-reducing Laemmli buffer and subsequently analyzed by Western blotting.

Immunofluorescence confocal microscopy

Immunostaining was performed according to methods previously described (Hasegawa et al., 2010). The primary Abs used included anti-VPS35 (GeneTex) and anti-CI-MPR (Epitomics) Abs. Positive immunostainings were detected using Alexa 488- and Alexa 568-conjugated secondary Abs (Molecular Probes/Life Technologies). Nuclei were counterstained with the far-red fluorescent DNA dye DRAQ7™ (CST) and were pseudocolored blue. Images were analyzed with a FluoView FV300 confocal laser microscope system equipped with HeNe-Green (543 nm), HeNe-Red (633 nm) and Ar (488 nm) laser units (Olympus, Tokyo, Japan). In multi-labeling experiments, images were collected using a single excitation for each wavelength separately, and were then merged using Fluoview image analysis software (version 4.1, Olympus).

Drosophila stocks

Fly culture and crosses were performed under standard conditions at 25 °C. The fly lines bearing *elav*-GAL4, *Act5c*-GAL4, *UAS*-EGFP, *UAS*-GFP dsRNA (*GFP*-RNAi), and *UAS-h[wt]-SNCA* transgenes were obtained from the Bloomington *Drosophila* Stock Center at Indiana University (BDSC, Bloomington, IN). The *VPS35* RNAi fly lines (#45570 and #22180, designated as *dVPS35* RNAi-1 and *dVPS35* RNAi-2, respectively) were provided by the Vienna Drosophila RNAi Center (VDRC, Vienna, Austria). Tg fly lines bearing the *GMR*-GAL4 have been described previously (Yamaguchi et al., 1999).

RT-PCR analysis

Total RNA was extracted from fly heads and their cDNA was synthesized with a SuperScript® III (Life Technologies). PCR amplification of dVPS35 was performed with 1 μl of cDNA solution and PrimeSTAR Max® DNA polymerase (Takara, Tokyo, Japan) with the following primer pairs: dVps35#2-F (5′-ATGGTTTGGATGACCAGGAGAAG-3′) in exon 1 and dVps35#2-R (5′-TCGTTCTCCTCAACCATCACATC-3′) in exon 3. Human αSYN was amplified using the set of primer pairs Syn-F (5′-TCGTGAGCGGAGAACTGGGAG-3′) and Syn-R (5′-TCAAGAAACTGGGAGCAAAGAT-3′) (Hasegawa et al., 2004). To normalize sample variations, the cDNA of ribosomal protein 49 (*rp49*), a housekeeping gene, was amplified using the primer pairs rp49-F (5′-AGCGCACCAAGCACTTCATCCGCCA-3′) and rp49-R (5′-GCGCACGTTGTGCACCAGGAACTTC-3′). After amplification, 10-ml aliquots were electrophoresed on 2.5% agarose gels, followed by photographic recording of the gels stained with ethidium bromide.

Immunohistochemistry

Sections of adult fly brain were immunostained according to the methods described previously (Feany and Bender, 2000). Briefly, 4-week-old adult flies were fixed in formalin and embedded in paraffin. To assess brain morphology, 5-μm frontal paraffin sections of heads were obtained and stained with hematoxylin and eosin. To evaluate the expression of human αSYN in the fly brain, anti-syn-1 monoclonal Ab (BD Bioscience) was applied at a 1:1000 dilution. Positive signals were detected by the avidin–biotin–peroxidase complex (Vectastain Elite ABC Kit, Vector Laboratories) method as described previously. The pictures were taken with a Biozero BZ-8000 digital microscope (Keyence, Tokyo, Japan). The numbers of αSYN-positive inclusions were counted per 15 × 15 μm^2 area in a defined area of the cortex (Kenyon cells) (Chen and Feany, 2005). Eight hemibrains were examined per genotype. The pooled data were statistically evaluated by a one-way ANOVA followed by a Bonferroni multiple comparison test.

Eye images

The eye phenotypes of 4-week-old anesthetized flies were evaluated. A minimum of 25 flies were evaluated for each genotype and conditions. Scanning electron microscopic images were obtained using a Miniscope TM-1000 (Hitachi, Tokyo, Japan). For the quantification of intact bristle numbers, a high-resolution image of a compound eye was printed, and the maximal visible surface was delimited (usually 300–500 ommatidia). The number of visible interommatidial bristles was counted and divided by the total number of ommatidia (Hilgers et al.,

2010). At least 10 eyes were analyzed for each genotype. The pooled data were statistically analyzed by a one-way ANOVA followed by a Bonferroni multiple comparison test.

Climbing assay

The climbing assay was performed, with slight modifications, according to published protocols (Feany and Bender, 2000). Ten to 20 male flies were placed into a conical glass tube (length, 15 cm; diameter, 2.5 cm) without anesthesia. Ten seconds after being tapped to the bottom of the tube, the number of flies in each vertical area was counted and scored as follows: score of 0 (0–2 cm), 1 (2–3.9 cm), 2 (4–5.9 cm), 3 (6–7.9 cm), 4 (8–9.9 cm), or 5 (10–15 cm). Five trials were performed in each group at 20 s intervals and the climbing index was calculated as follows: each score multiplied by the number of flies was divided by the total number of flies, and the mean score of each trial was calculated. The results are presented as the means ± standard errors of the scores obtained in 5–7 independent experiments. All climbing assay experiments were conducted at 25 °C. Pooled data from at least five independent experiments were statistically analyzed using a two-way ANOVA with a Bonferroni multiple comparison test.

Results

VPS35 RNAi alters CI-MPR distribution and impairs maturation of CTSD

The RNAi-mediated silencing of retromer subunits, such as VPS26 and Rab7, prevents the retrieval of unoccupied CI-MPR from endosomes to the TGN, leading to the lysosomal turnover of CI-MPR and a decrease in the cellular level of lysosomal hydrolases (Rojas et al., 2008). To determine whether the depletion of VPS35 also affects the intracellular distribution of CI-MPR, we downregulated VPS35 in HEK293 cells using two different siRNAs (#1 and #2) targeting *VPS35*. Consistent with previous findings (Rojas et al., 2008), the punctate signals of CI-MPR in cells expressing a normal level of endogenous VPS35 were preferentially localized in the perinuclear space, in which the TGN and late endosomes are usually located (Fig. 1A, left inset). In contrast, the CI-MPR signals in the VPS35-deficient cells were strikingly decreased and showed a more dispersed distribution in the periphery (Fig. 1A, right inset). As shown in Fig. 1B, human CTSD is first synthesized as pre-pro-CTSD, which is further converted to pro-CTSD (52 kDa), by the removal of the signal peptide, in the endoplasmic reticulum. The transport of pro-CTSD from the Golgi to the downstream acidic compartments is mainly mediated by the M6P pathway, i.e., the M6P residues on pro-CTSD are recognized by CI-MPR in the TGN, which segregates CTSD into transport vesicles that are delivered to the late endosomes and lysosomes. In late endosomes, pro-CTSD is processed to an intermediate form (48 kDa) and subsequently converted to mature CTSD (34 kDa) in lysosomes (Laurent-Matha et al., 2006). We confirmed that the ablation of the VPS35 component of the retromer by RNAi in HEK293 cells caused a considerable increase in intracellular pro-CTSD (indicated by an *asterisk*), whereas the amount of intracellular mature CTSD (indicated by an arrowhead) was markedly decreased. Notably, these changes were accompanied by a concomitant increase in pro-CTSD in the culture medium (Fig. 1C and D). The reduction in CI-MPR expression observed in VPS35-deficient cells implies a rerouting of CI-MPR to the lysosome for degradation, which is indicative of retromer dysfunction. As suggested by previous studies, the level of VPS26, a known interaction partner of VPS35, was substantially decreased in VPS35-silenced cells. The aberrant processing of CTSD in VPS35-deficient cells was further confirmed by an enzymatic assay showing that the activity of CTSD in VPS35 siRNA-treated cells was significantly lower than that in scrambled siRNA-treated cells (Fig. 1E).

VPS35 downregulation induces the αSYN accumulation in parallel with the reduction of mature CTSD in late endosomes and lysosomes

To examine whether CTSD effectively degrades αSYN in cultured cells, we over-expressed human CTSD in HEK293 cells that constitutively expressed human αSYN. When CTSD was highly over-expressed (3 μg of plasmid DNA per transfection) for 48 h, the level of mature CTSD was increased and the signal intensity of the monomeric, full-length αSYN (17 kDa) was significantly decreased (Fig. 2A, upper panel). Notably, in the presence of the protein synthesis inhibitor cycloheximide, the effect of CTSD on αSYN degradation was augmented and the amount of αSYN was significantly decreased in proportion to the dosage of CTSD expression (Fig. 2A, lower panel). Because pro-CTSD has a relatively long half-life (3–6 h) compared to αSYN (1.84 ± 0.16 h) (Bennett et al., 1999; Capony et al., 1989), it is likely that the cycloheximide blockage of protein synthesis did not affect CTSD levels dramatically. In agreement with a previous report (Cullen et al., 2009), the decrement in the αSYN monomer level was not accompanied by the appearance of low-molecular-weight αSYN fragments even with a long exposure of the immunoblot to the synuclein-1 Ab, which had previously shown reactivity with C-terminally truncated αSYN fragments *in vivo*. We used an MTT (3-(4,5-dimethylthiazo-2-yl)-2,5-diphenyltetrazolium bromide) assay to confirm that the observed effect of CTSD on lowering αSYN expression was not caused by impaired viability of the transfected cells (data not shown). In the second set of experiments, we examined whether the reduction in mature CTSD in response to *VPS35* knockdown altered the expression level of αSYN in the HEK293 cells stably expressing HA-tagged αSYN. Remarkably, the loss of VPS35 induced the accumulation of cellular HA-αSYN concomitant with incorrect processing of CTSD (Fig. 2B). The relative decrease in MPR in VPS35-depleted cells was interpreted as compromised retromer recruitment. Because CTSD is only active in an acidic environment, such as in late endosomes and lysosomes, serial fractionation was conducted to clarify the subcellular distribution of HA-αSYN in the *VPS35*-silenced cells. Thirty-six hours after silencing, the cells were harvested and sequentially fractionated into cytosol, endosome, and lysosome fractions. All samples were subjected to an immunoblot analysis, and the relative purity of the fractions was assessed using Abs directed against specific markers including Heat shock protein 90 (HSP90; cytosol), Rab5 (early endosome), and lysosome-associated membrane protein-2 (LAMP-2; lysosome). The results, shown in Fig. 2C, revealed that after silencing *VPS35*, the expression level of CI-MPR was slightly decreased in the endosomes but simultaneously increased downstream, in the lysosomal compartment. It

Fig. 1. Silencing of VPS35 caused a reduction in CI-MPR distribution and impaired maturation of CTSD. (A) The punctate signals of CI-MPR (red) in HEK293 cells expressing a normal level of endogenous VPS35 (green) were preferentially localized in the perinuclear space (left inset). In contrast, the signal of CI-MPR in VPS35-deficient cells was strikingly decreased and had a more dispersed distribution throughout the cell (right inset). White dotted lines show the contour of the cells. Nuclei were counterstained with DRAQ7. Scale bar: 10 μm. (B) Schematic diagram of the maturation process of CTSD. Human CTSD is first synthesized as pre-pro-CTSD, which is converted to pro-CTSD (52 kDa) by the removal of the signal peptide in the endoplasmic reticulum. The transport of pro-CTSD from the Golgi to the downstream acidic compartments is mainly mediated by the CI-MPR. In late endosomes, pro-CTSD is processed to an intermediate form (48 kDa) and subsequently converted to mature CTSD (34 kDa) in lysosomes. (C) The aberrant processing of CTSD in VPS35-deficient cells. The silencing of VPS35 by two different siRNAs (#1 and #2) in HEK293 cells caused a striking increase in the intracellular pro-CTSD (asterisk), whereas the amount of intracellular mature CTSD (arrowhead) was markedly decreased. This finding was accompanied by a concomitant increase in pro-CTSD in the medium. The left inset is CTSD with a longer exposure time. The reduction in CI-MPR expression observed in VPS35-deficient cells is indicative of retromer dysfunction. Note that the level of VPS26, another component of the retromer, was substantially decreased in VPS35-silenced cells. α-Tubulin and BSA were used as the internal controls for the total cell lysate and the medium, respectively. Representative blots from five independent experiments are presented. (D) The ratio of the densitometric values of mature/pro-CTSD both in cells and the medium is presented. Data are expressed as the means ± standard errors. $^{\dagger}p < 0.05$ and $^{\ddagger}p < 0.01$ (one-way ANOVA followed by Dunnett's test; $n = 5$). (E) The activity of CTSD in VPS35-specific siRNA (#1 and #2)-treated cells significantly declined compared to the activity in scrambled siRNA-treated cells. Data are expressed as the means ± standard errors. $^{\#}p < 0.05$ (one-way ANOVA followed by Dunnett's test; $n = 5$).